CHAPTER 7

Method of Finite Differences

Many engineering problems in electromagnetics may be formulated as partial differential equations (PDE). This may include electrostatic problems formulated as Laplace or Poisson equations; or dynamic problems such as wave equations. Only a few of the useful geometries can be solved using analytical methods. Computers may be used to directly solve the boundary value problems to include the effects of dielectric inhomogeneities and irregular boundary. For the direct solution of PDE, the differential equations should be expressed in a form suitable for computers. The difference form of the derivatives is most suitable and can be programmed in a computer. The method of finite differences is based on the solution of PDE when expressed in finite difference form. This method is least analytical and therefore easy to follow. It is a versatile method, but its efficiency is poor. This method is taught to the undergraduate students as a part of numerical solution of PDE. With this preparation, the students can be easily introduced to the computational methods. A very good exposition of finite difference method (FDM) with its applications in electromagnetics is available in [1–4].

7.1 Finite Difference Approximations

The method of finite differences involves the following major steps:

1. The difference form of the derivatives is used to express the differential equation in the finite difference form, and the governing equation obtained.
2. The device is discretized in the form of cells, creating a number of nodes.
3. The finite difference form of the differential equation is applied at each and every node creating a number of linear simultaneous equations.
4. The set of simultaneous equations is solved to determine the unknown nodal potential.
5. The potential distribution may be used to derive engineering-important characteristics like capacitance, characteristic impedance, cutoff wavelength, resonant frequency, and so on.

7.1.1 Difference Form of the First Derivative

Consider the function $f(x)$ in Figure 7.1. The derivative of the function at x_0 is defined as

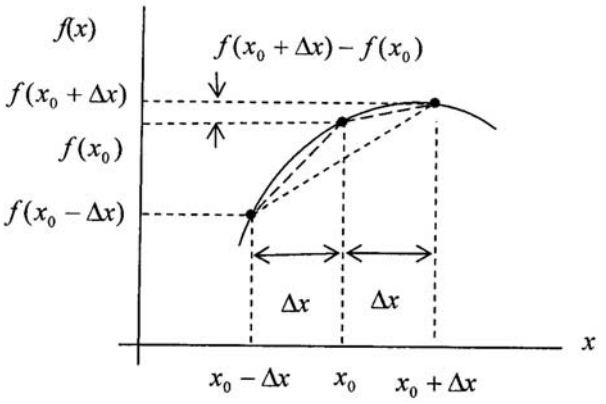

Figure 7.1 Illustration for the difference form of the first derivative.

$$f'(x_0) = \underset{x \to x_0}{lt} \frac{f(x) - f(x_0)}{x - x_0} \tag{7.1}$$

Although this definition is exact, it is not computer friendly. The value of the function might not be available for all values of x, but only at discrete points. For this reason, we may *approximate* the derivative as follows:

$$f'(x_0) = \underset{\Delta x \to 0}{lt} \frac{f(x_0 + \Delta x) - f(x_0)}{\Delta x} \approx \frac{f(x_0 + \Delta x) - f(x_0)}{\Delta x} \tag{7.2a}$$

where Δx is the discretization length along x. Expression (7.2a) is called the *forward difference approximation* of the derivative. This form of derivative is approximate when Δx is nonzero. Another possibility is

$$f'(x_0) = \underset{\Delta x \to 0}{lt} \frac{f(x_0) - f(x_0 - \Delta x)}{\Delta x} \approx \frac{f(x_0) - f(x_0 - \Delta x)}{\Delta x} \tag{7.2b}$$

This expression is called the *backward difference approximation* of the derivative. Still another possibility is

$$f'(x_0) = \underset{\Delta x \to 0}{lt} \frac{f(x_0 + \Delta x) - f(x_0 - \Delta x)}{2\Delta x} \approx \frac{f(x_0 + \Delta x) - f(x_0 - \Delta x)}{2\Delta x} \tag{7.2c}$$

This equation is called the *central difference approximation* of the derivative.

The three different forms of the first derivative are found to give varying amount of approximation to the derivative for nonzero value of Δx. Let us first determine the approximation involved. Consider the Taylor series expansion of $f(x)$ about the point x_0,

$$f(x_0 \pm \Delta x) = f(x_0) \pm \Delta x \left.\frac{df}{dx}\right|_{x_0} + \frac{(\Delta x)^2}{2} \left.\frac{d^2f}{dx^2}\right|_{x_0} \pm \frac{(\Delta x)^3}{3!} \left.\frac{d^3f}{dx^3}\right|_{x_0} + \ldots \quad (7.3)$$

Using this expansion in the forward difference approximation (7.2a) gives

$$\frac{f(x_0 + \Delta x) - f(x_0)}{\Delta x} = \left.\frac{df}{dx}\right|_{x_0} + \frac{\Delta x}{2} \left.\frac{d^2f}{dx^2}\right|_{x_0} + \frac{(\Delta x)^2}{3!} \left.\frac{d^3f}{dx^3}\right|_{x_0} + \ldots \quad (7.4a)$$

The second, third, and subsequent terms on the right side represent the error terms for $\Delta x \neq 0$. Similarly, the backward difference approximation gives

$$\frac{f(x_0) - f(x_0 - \Delta x)}{\Delta x} = \left.\frac{df}{dx}\right|_{x_0} - \frac{\Delta x}{2} \left.\frac{d^2f}{dx^2}\right|_{x_0} + \frac{(\Delta x)^2}{3!} \left.\frac{d^3f}{dx^3}\right|_{x_0} + \ldots \quad (7.4b)$$

Adding (7.4a) and (7.4b) gives the following expression for the central difference approximation [1–7]:

$$\frac{f(x_0 + \Delta x) - f(x_0 - \Delta x)}{2\Delta x} = \left.\frac{df}{dx}\right|_{x_0} + \frac{(\Delta x)^2}{3!} \left.\frac{d^3f}{dx^3}\right|_{x_0} + \ldots \quad (7.4c)$$

It may be observed that the error in finite difference approximation is of the order of Δx in (7.4a) and (7.4b), and it is of the order of $(\Delta x)^2$ for the central difference approximation, (7.4c). The error is lower in case of (7.4c), because $\Delta x < 1$. The error is called discretization error and may be reduced for the same step size by using more nodal values about the central node [4]. Care must be exercised in applying the higher-order approximations in finite difference methods because the resulting expression may represent higher order derivative than the intended second order derivative and may lead to spurious solution.

7.1.2 Difference Form of the Second Derivative

Solutions of Laplace, Poisson, or wave equations, using the method of finite differences, require the knowledge of the difference form of the second derivative and the associated errors. In order to find the difference approximation for d^2f/dx^2, let us consider three nodes in the grid at x_0, $x_0 + \Delta x$, and $x_0 - \Delta x$, as shown in Figure 7.1. Using the Taylor expansion (7.3) gives

$$f(x_0 + \Delta x) + f(x_0 - \Delta x) = 2f(x_0) + (\Delta x)^2 \left.\frac{d^2f}{dx^2}\right|_{x_0} + 2\frac{(\Delta x)^4}{4!} \left.\frac{d^4f}{dx^4}\right|_{x_0} + \ldots$$

or

$$\left.\frac{d^2f}{dx^2}\right|_{x_0} = \frac{f(x_0+\Delta x) - 2f(x_0) + f(x_0-\Delta x)}{(\Delta x)^2} - \frac{(\Delta x)^2}{12}\left.\frac{d^4f}{dx^4}\right|_{x_0} + \ldots \quad (7.5)$$

It is obvious from above that if d^2f/dx^2 is approximated as

$$\left.\frac{d^2f}{dx^2}\right|_{x_0} \approx \frac{f(x_0+\Delta x) - 2f(x_0) + f(x_0-\Delta x)}{(\Delta x)^2} \quad (7.6a)$$

the error in (7.6a) is of the order of Δx^2; that is, $O(\Delta x^2)$. Similarly, for the function $f(x, y)$ of two independent variables x and y, the derivative $\partial^2 f/\partial y^2$ may be approximated as

$$\frac{\partial^2 f}{\partial y^2} \approx \frac{f(x_0, y_0+\Delta y) - 2f(x_0, y_0) + f(x_0, y_0-\Delta y)}{(\Delta y)^2} \quad (7.6b)$$

7.1.3 Difference Form of Laplace and Poisson Equations

Let us consider the solution of electrostatic problems governed by the Laplace equation,

$$\nabla^2 \varphi = 0 \quad (7.7)$$

or

$$\frac{\partial^2 \varphi}{\partial x^2} + \frac{\partial^2 \varphi}{\partial y^2} = 0 \qquad \text{in two-dimensions} \quad (7.8)$$

To derive the difference form of (7.8), let us consider four nodes surrounding the central node in a square grid with node spacing h as shown in Figure 7.2. The value of the function $\varphi(x, y)$ at the surrounding nodes are φ_1, φ_2, φ_3, and φ_4. Using (7.5) for the second order derivative along the x-direction, we have

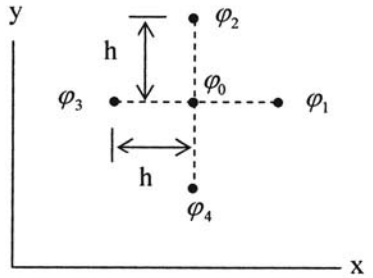

Figure 7.2 Nodes in a square grid.

$$\frac{\partial^2 \varphi}{\partial x^2} = \frac{\varphi_1 - 2\varphi_0 + \varphi_3}{h^2} - \frac{h^2}{12}\frac{\partial^4 \varphi}{\partial x^4} + \ldots \tag{7.9a}$$

Similarly, the second order derivative along the y-direction is given by

$$\frac{\partial^2 \varphi}{\partial y^2} = \frac{\varphi_2 - 2\varphi_0 + \varphi_4}{h^2} - \frac{h^2}{12}\frac{\partial^4 \varphi}{\partial y^4} + \ldots \tag{7.9b}$$

Add (7.9a) and (7.9b), use Laplace equation (7.8), and multiply throughout by h^2 to obtain

$$\varphi_0 = \frac{1}{4}(\varphi_1 + \varphi_2 + \varphi_3 + \varphi_4) - \frac{h^4}{48}\left[\frac{\partial^4 \varphi}{\partial x^4} + \frac{\partial^4 \varphi}{\partial y^4}\right] + \ldots \tag{7.10}$$

If the value at the central node is approximated by the first term on the right side, the last term contributes to the error due to the nonzero value of h. The error is of the order of h^4. We may approximate (7.10) as

$$\varphi_0 \approx \frac{1}{4}(\varphi_1 + \varphi_2 + \varphi_3 + \varphi_4) \tag{7.11}$$

Equation (7.11) may be generalized for any node (i, j) as

$$\varphi(i, j) \approx \frac{1}{4}[\varphi(i+1, j) + \varphi(i, j+1) + \varphi(i-1, j) + \varphi(i, j-1)] \tag{7.12}$$

Equation (7.12) is the governing equation for the finite difference analysis of Laplace equation. It is also called the five-point finite difference approximation of Laplace equation. It implies that the potential at the central node is the average of the potentials at the four neighboring nodes, and *may be used to determine the potential distribution for a problem satisfying Laplace equation*. For this, (7.12) is written for each and every node in the problem space. Arranging these equations gives a set of simultaneous equations which can be solved for the unknowns. Some of these equations may be eliminated by the boundary conditions. The set of equations is singular unless the potential of at least one node is specified.

The Poisson equation defined as

$$\frac{\partial^2 \varphi}{\partial x^2} + \frac{\partial^2 \varphi}{\partial y^2} = \rho(x, y) \tag{7.13}$$

may also be discretized in the same way as the Laplace equation to obtain the following approximate expression for the potential at the central node:

$$\varphi_0 \approx \frac{1}{4}(\varphi_1 + \varphi_2 + \varphi_3 + \varphi_4 - \rho(x_0, y_0)h^2) \tag{7.14}$$

For a *rectangular* grid with node spacing Δx along the x-direction and Δy along the y-direction, the discretized form of the Poisson equation for the potential at the central node at (i, j) may be written as

$$\varphi_{i,j}\left(\frac{\Delta y}{\Delta x}+\frac{\Delta x}{\Delta y}\right) \approx \frac{1}{2}\left[\frac{\Delta y}{\Delta x}(\varphi_{i+1,j}+\varphi_{i-1,j})+\frac{\Delta x}{\Delta y}(\varphi_{i,j+1}+\varphi_{i,j-1})-\rho(x_i, y_j)\,\Delta x\,\Delta y\right] \tag{7.15}$$

This expression reduces to (7.14) for $\Delta x = \Delta y = h$.

Quiz 7.1. The discretization error associated with the approximation $f'\left(x_0+\frac{h}{2}\right) \approx \frac{f(x_0+h)-f(x_0)}{h}$ is of the order of

(a) h
(b) h^2
(c) None of the above

Answer. (b). The given expression is central difference approximation about the point $(x_0 + h/2)$. Or expand $f(x_0 + h)$ and $f(x_0)$ about $f(x_0 + h/2)$.

Example 7.1. The geometry in Figure 7.3 consists of an infinitely long square metal pipe with insulation at the corners so that the different faces of the pipe can be raised to different potentials. We would like to determine the potential distribution, V inside this pipe.

Since the geometry is invariant along the length, we expect the potential distribution also to be invariant along the length. Therefore, the problem reduces to a two-dimensional problem in the cross-sectional plane, xy.

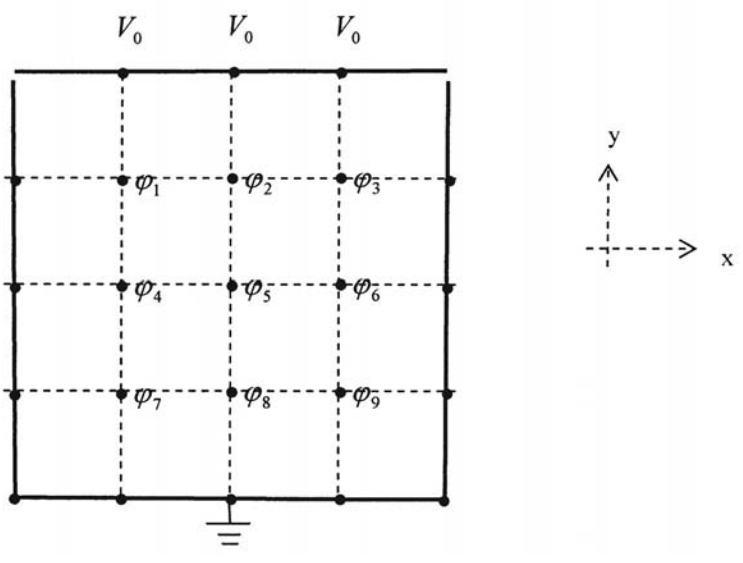

Figure 7.3 Geometry of a square pipe showing grid lines, nodes, and boundary conditions.

The inside of the pipe is discretized in square cells of size $h \times h$. The nodes are introduced at the crossings of grid lines. There are 23 nodes in Figure 7.3, with 9 nodes distributed inside the pipe and 14 on the surfaces. The nodes on the surfaces are called fixed nodes because the potential on these nodes is fixed by the boundary conditions. The internal nodes are called free nodes because the potential at these nodes is free to adjust to satisfy the boundary conditions. The governing Laplace equation should be satisfied at each and every point of the geometry. Let us apply the discretized version of Laplace equation, (7.12), at the various nodes of Figure 7.3. Next the boundary conditions due the voltage at the four conducting strips constituting the pipe are applied. Let these potentials be: 0V, 0V, 0V, and V_0. Since the potentials on the nodes residing at the four surfaces is specified, we need not write (7.12) for these nodes. This way we are left with only nine nodes, distributed inside the pipe, at which the potential is to be determined. The symmetry of the pipe and the boundary conditions about the mid-plane parallel to the y-axis indicate that $\varphi_1 = \varphi_3$, $\varphi_4 = \varphi_6$, and $\varphi_7 = \varphi_9$, leaving six unknowns, φ_1, φ_2, φ_4, φ_5, φ_7, and φ_8. Implementing (7.12) at the six nodes gives the following equations:

$$4\varphi_1 = 0 + V_0 + \varphi_2 + \varphi_4 \tag{7.16a}$$

$$4\varphi_2 = \varphi_1 + V_0 + \varphi_1 + \varphi_5, \qquad \text{because } \varphi_3 = \varphi_1 \tag{7.16b}$$

$$4\varphi_4 = 0 + \varphi_1 + \varphi_5 + \varphi_7 \tag{7.16c}$$

$$4\varphi_5 = \varphi_4 + \varphi_2 + \varphi_4 + \varphi_8, \qquad \text{because } \varphi_6 = \varphi_4 \tag{7.16d}$$

$$4\varphi_7 = 0 + \varphi_4 + \varphi_8 + 0 \tag{7.16e}$$

$$4\varphi_8 = \varphi_7 + \varphi_5 + \varphi_7 + 0, \qquad \text{because } \varphi_9 = \varphi_7 \tag{7.16f}$$

The above set of equations may be expressed in the form of a matrix equation with known quantities transferred to the right side. One obtains

$$\begin{bmatrix} 4 & -1 & -1 & 0 & 0 & 0 \\ -2 & 4 & 0 & -1 & 0 & 0 \\ -1 & 0 & 4 & -1 & -1 & 0 \\ 0 & -1 & -2 & 4 & 0 & -1 \\ 0 & 0 & -1 & 0 & 4 & -1 \\ 0 & 0 & 0 & -1 & -2 & 4 \end{bmatrix} \begin{bmatrix} \varphi_1 \\ \varphi_2 \\ \varphi_4 \\ \varphi_5 \\ \varphi_7 \\ \varphi_8 \end{bmatrix} = \begin{bmatrix} V_0 \\ V_0 \\ 0 \\ 0 \\ 0 \\ 0 \end{bmatrix} \tag{7.17}$$

Solution Methods for the Set of Simultaneous Equations

The application of the finite difference method to the Laplace equation has led to a set of simultaneous equations as described above. Their efficient solution is a major problem in itself. For matrices of small sizes, one may use a direct approach in the form of matrix inversion or by using the Gauss elimination method (see Appendix A). The indirect or iterative methods are more efficient for matrices which are diagonally dominant, sparse, and large. The above matrix is diagonally dominant and sparse.

Iterative Methods

An iterative method is one in which a first approximation is used to calculate a second approximation, which in turn is used to calculate the third approximation, and so on until a specified tolerance is attained. The three common iterative methods are: Jacobi, Gauss-Seidel, and successive over-relaxation (SOR). We discuss the implementation of SOR next.

The value at the free nodes may be set equal to zero to start with in the absence of any educated guess. Now consider node φ_1 and apply (7.12) as in (7.16a). We raster scan, from top to bottom and left to right, through all the nodes at which the potential is to be determined. This procedure is iterated a number of times such that the potential at a node does not change much in the next iteration and is within a specified tolerance. For example, if the specified tolerance is 1%, then the iteration is continued until

$$\left|\varphi_{i,j}^{n+1} - \varphi_{i,j}^{n}\right| < \left|0.01\varphi_{i,j}^{n}\right| \tag{7.18}$$

where the superscript n denotes the iteration number. The problem of Example 7.1 was solved using this method. It was found that after six iterations

$$\begin{aligned} &\varphi_1 = 0.4274V_0,\ \varphi_2 = 0.5256V_0,\ \varphi_4 = 0.1863V_0 \\ &\varphi_5 = 0.2488V_0,\ \varphi_7 = 0.0708V_0,\ \varphi_8 = 0.0976V_0 \end{aligned} \tag{7.19}$$

The accuracy of this solution can be determined by comparing it with the values given by the exact solution [8],

$$\varphi(x, y) = \frac{2V_0}{\pi} \sum_{n=1}^{\infty} [1 - (-1)^n] \frac{\sinh\left(\frac{n\pi y}{a}\right)}{n \sinh\left(\frac{n\pi b}{a}\right)} \sin\left(\frac{n\pi x}{a}\right) \tag{7.20}$$

where a is the width and b is the height of the pipe. The values obtained from (7.20) are as follows:

$$\begin{aligned} &\varphi_1 = 0.4320V_0,\ \varphi_2 = 0.5405V_0,\ \varphi_4 = 0.1820V_0 \\ &\varphi_5 = 0.2500V_0,\ \varphi_7 = 0.0680V_0,\ \varphi_8 = 0.0954V_0 \end{aligned}$$

The difference between the analytical solution and the finite difference solution is found to be about 4%. The error can be reduced by reducing the cell size h, that is, by increasing the number of nodes inside the pipe.

Successive Over-Relaxation (SOR)

The simplistic structure of the FDM needs very fine discretization for accurate results. The number of nodes, therefore, becomes very large, resulting in large computer storage and the number of iterations. The iterations can be reduced by using SOR. The relaxation formula for the new value $\varphi_{i,j}^{n+1}$ in terms of the old value $\varphi_{i,j}^{n}$ is given by

$$\varphi_{i,j}^{n+1} = \varphi_{i,j}^{n} + \Omega_0 R_{i,j}^{n+1} \tag{7.21a}$$

where Ω_0 is the relaxation factor which determines the rate of convergence and $R_{i,j}^{n+1}$ is the residual at each node and is defined as

$$R_{i,j}^{n+1} = \frac{1}{4}\left(\varphi_{i+1,j}^{n} + \varphi_{i-1,j}^{n+1} + \varphi_{i,j-1}^{n+1} + \varphi_{i,j+1}^{n}\right) - \varphi_{i,j}^{n} \tag{7.21b}$$

It may be noted that updated nodal values are included for the nodes surrounding node (i, j). The residual $R_{i,j}^{n+1}$ may be regarded as a correction, which must be added to $\varphi_{i,j}^{n}$ to make it nearer to the correct value. As convergence to the correct value is approached, $R_{i,j}^{n+1}$ tends to zero. The process of successive correction of the nodal value for $\Omega_0 = 1$ is called relaxation. An optimum value of Ω_0 may reduce the number of iterations considerably. The optimum value of Ω_0 is determined by trial and error and is found to lie in general between 1 and 2 [3]. For the rectangular cells the optimum relaxation factor is given by the root of the quadratic equation [9]

$$\Omega_0^2 r^2 - 16\Omega_0 + 16 = 0 \tag{7.22a}$$

where $r = \cos(\pi/N_x) + \cos(\pi/N_y)$, and N_x and N_y are the number of cells per unit length along the x- and y-directions, respectively. Therefore,

$$\Omega_0 = \frac{8 - \sqrt{64 - 16r^2}}{r^2} \tag{7.22b}$$

It has been found that the optimum value Ω_0 holds for sufficiently large node density.

The trough problem of Example 7.1 is now analyzed for a large number of nodes. For this, a software *trough.m* is developed. This software employs an iterative method for the solution of the matrix equation. SOR is used to improve efficiency. The number of iterations as a function of Ω for 1% tolerance is plotted in Figure 7.4. The node density $N = N_x = N_y = 30$.

The software determines the optimum value of Ω from the number of iterations and compares this value with the value given by (7.22b). The optimum value in this case is found to be 1.8170, whereas the analytical value is 1.8107. The number of iterations required is 14. The equipotential contours are plotted in Figure 7.5. As expected, the potential decreases away from the top plate and is symmetric about the mid-plane because of the symmetry of the boundary conditions.

Exercise. Determine the optimum value of Ω as a function of node density for square cells using software *trough.m*. Assume $N > 20$ and tolerances of 1% and 0.1%. Compare the values with those obtained from (7.22b).

Quiz 7.2. In Example 7.1, the potential distribution is symmetric about the y-axis. It is due to:

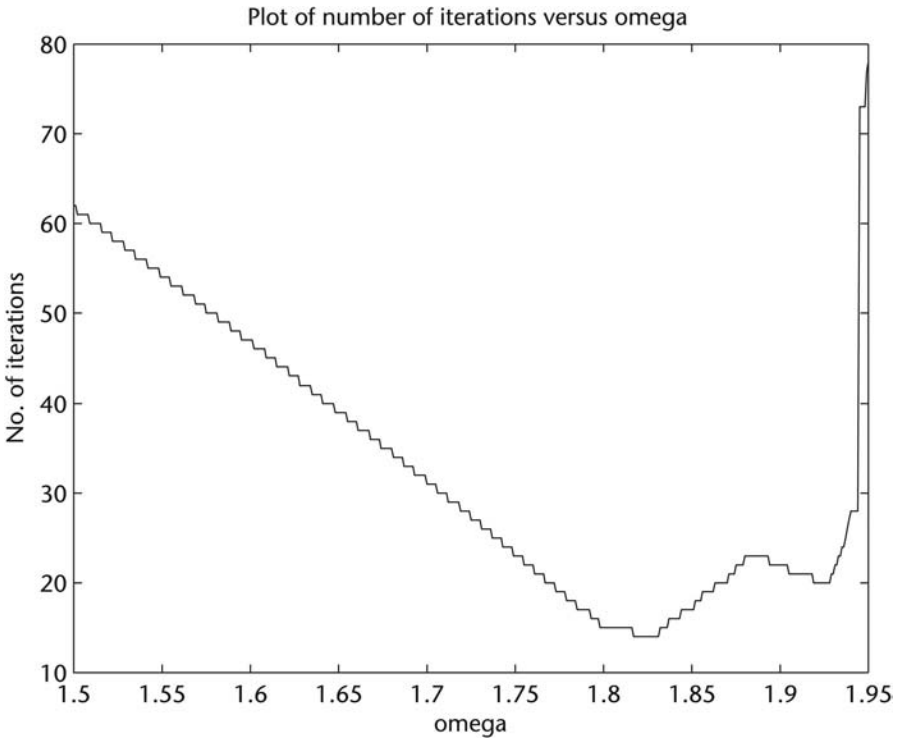

Figure 7.4 Plot of number of iterations as a function of relaxation factor, Ω. The node density *N*: 30 and tolerance: 1%.

(a) The symmetry of the trough about the y-axis
(b) The symmetry of the boundary conditions about the y-axis
(c) Both (a) and (b)
(d) None of the above

Prove your point through simulations after making suitable changes in the problem.

Answer. (c).

Quiz 7.3. In Example 7.1, the potential distribution depends on the discretization size h. In other words, the potential distribution changes with change in the value of h. Also, the boundary condition is satisfied at different number of points for different values of h. The change in potential value at a common node is:

(a) Due to the change in discretization error
(b) Due to the modified boundary conditions
(c) Due to both (a) and (b)
(d) None of the above

Please choose the correct entries and explain why.

Answer. (c).

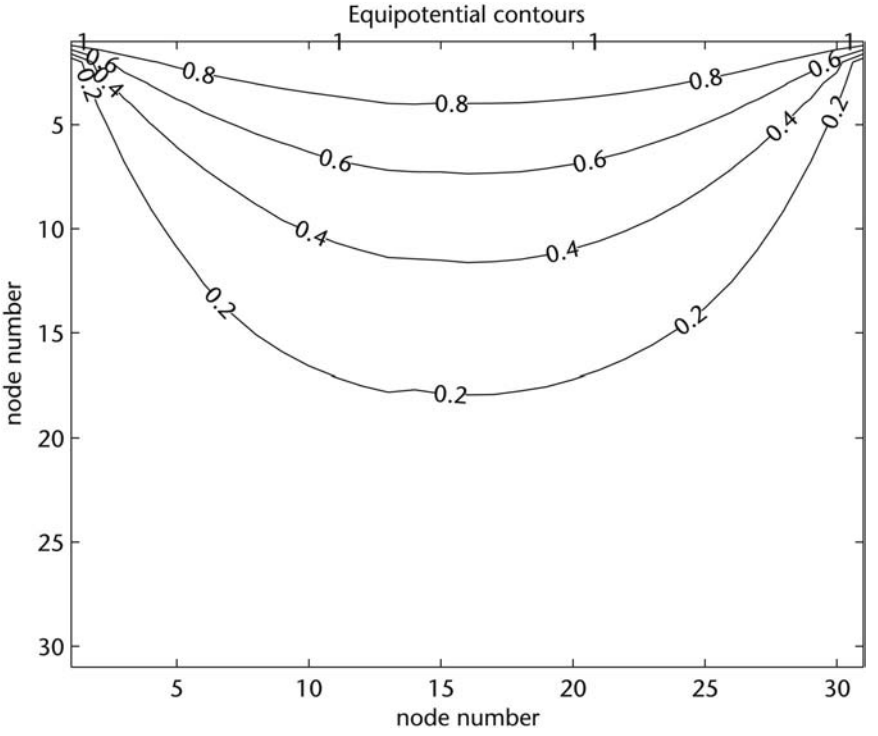

Figure 7.5 Equipotential contours for the trough. Node density N: 30, tolerance: 1%.

7.2 Treatment of Interface and Boundary Conditions

One of the reasons why we use computational methods is the ease with which the material inhomogeneity and the complicated geometries can be handled. These may give rise to nodes at the dielectric interface, nodes at the corner, and nodes on the edge [1]. The finite difference equations for these nodes are different from the equation for the node in the interior. Let us first consider the nodes on an interface between two dielectrics.

7.2.1 Nodes on the Interface

The dielectric interface occurs in geometries with dielectric inhomogeneities such as planar transmission lines and partially filled waveguides. The analysis of these geometries invariably involves placing nodes on the interface. Consider Figure 7.6 with nodes at the interface of two dielectrics ϵ_1 and ϵ_2. Let us determine the finite difference equation for the central node with assumed potential φ_0. If there is no charge on the interface, then the application of Gauss's law will give rise to an equation for φ_0 in terms of the potentials at the nodes in the neighborhood. Using the dotted line cell as the Gaussian surface, we determine the flux leaving this surface. The Gauss law for the electric field states that the electric flux leaving a Gaussian surface is equal to the free charge enclosed by the surface [2]; that is,

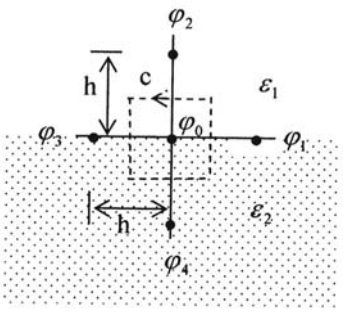

Figure 7.6 Nodes at the interface of two dielectrics.

$$\oiint_s \epsilon \mathbf{E}.\mathbf{ds} = q = 0 \tag{7.23}$$

Since there is no *free* charge enclosed by the Gaussian surface, q is set equal to zero. Substituting $\mathbf{E} = -\nabla\varphi$ gives

$$-\oint_c \epsilon \nabla\varphi.\mathbf{dc} = 0 \tag{7.24}$$

where the two-dimensional closed surface has been replaced by the closed contour c in Figure 7.6. Denoting the derivative of φ on the contour by $\partial\varphi/\partial n$, we obtain

$$-\oint_c \epsilon \frac{\partial\varphi}{\partial n}\, dc = 0 \tag{7.25}$$

where n is the unit *outward* normal to the contour. The flux leaving the right side of the contour is

$$\psi_R = \epsilon_1 \frac{\varphi_1 - \varphi_0}{h}\frac{h}{2} + \epsilon_2 \frac{\varphi_1 - \varphi_0}{h}\frac{h}{2} \tag{7.26a}$$

Similarly, the flux leaving the left side is

$$\psi_L = \epsilon_1 \frac{\varphi_3 - \varphi_0}{h}\frac{h}{2} + \epsilon_2 \frac{\varphi_3 - \varphi_0}{h}\frac{h}{2} \tag{7.26b}$$

The flux leaving the top side is

$$\psi_T = \epsilon_1 \frac{\varphi_2 - \varphi_0}{h} h \tag{7.26c}$$

and the flux leaving the bottom side is

$$\psi_B = \epsilon_2 \frac{\varphi_4 - \varphi_0}{h} h \tag{7.26d}$$

Setting the total flux leaving the Gaussian surface to zero, we obtain

$$\epsilon_1 \frac{\varphi_1 - \varphi_0}{h} \frac{h}{2} + \epsilon_2 \frac{\varphi_1 - \varphi_0}{h} \frac{h}{2} + \epsilon_1 \frac{\varphi_3 - \varphi_0}{h} \frac{h}{2} + \epsilon_2 \frac{\varphi_3 - \varphi_0}{h} \frac{h}{2} + \epsilon_1 \frac{\varphi_2 - \varphi_0}{h} h + \epsilon_2 \frac{\varphi_4 - \varphi_0}{h} h = 0 \tag{7.27}$$

Rearranging the terms gives

$$\frac{\epsilon_1 + \epsilon_2}{2} \varphi_0 = \frac{1}{4} \left(\frac{\epsilon_1 + \epsilon_2}{2} \varphi_1 + \epsilon_1 \varphi_2 + \frac{\epsilon_1 + \epsilon_2}{2} \varphi_3 + \epsilon_2 \varphi_4 \right) \tag{7.28}$$

It may be noted that (7.28) reduces to (7.11) for $\epsilon_1 = \epsilon_2$. Also, (7.28) can be written down by inspection from (7.11) if the average of the permittivity surrounding the node is used as the permittivity multiplier; that is, $(\epsilon_1 + \epsilon_2)/2$ for the nodes on the interface and the appropriate ϵ value for the nodes in the medium. If the dielectric interface occurs along the line joining the nodes 2 and 4, the expression for φ_0 in this case may be obtained from the simple permutation of (7.28) [1].

7.2.2 Dielectric Inhomogeneity in One Quadrant About a Node

The geometry of dielectric inhomogeneity in one quadrant about a node is shown in Figure 7.7. Here, the dielectric ϵ_2 occupies the fourth quadrant of the Gaussian surface while the other three quadrants are occupied by ϵ_1. Using the procedure described in the last subsection, the total flux leaving the Gaussian surface is found to be

$$\epsilon_1 \frac{\varphi_1 - \varphi_0}{h} \frac{h}{2} + \epsilon_2 \frac{\varphi_1 - \varphi_0}{h} \frac{h}{2} + \epsilon_1 \frac{\varphi_2 - \varphi_0}{h} h + \epsilon_1 \frac{\varphi_3 - \varphi_0}{h} h + \epsilon_1 \frac{\varphi_4 - \varphi_0}{h} \frac{h}{2} + \epsilon_2 \frac{\varphi_4 - \varphi_0}{h} \frac{h}{2} = 0 \tag{7.29}$$

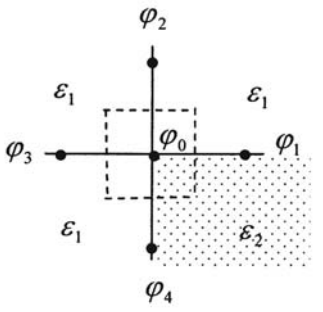

Figure 7.7 Node at the corner of dielectric inhomogeneity.

Rearranging (7.29) gives for the potential at the central node

$$\frac{3\epsilon_1 + \epsilon_2}{4}\varphi_0 = \frac{1}{4}\left(\frac{\epsilon_1 + \epsilon_2}{2}\varphi_1 + \epsilon_1\varphi_2 + \epsilon_1\varphi_3 + \frac{\epsilon_1 + \epsilon_2}{2}\varphi_4\right) \tag{7.30}$$

Again, (7.30) can be written down by inspection if the average permittivity surrounding the node is used in (7.11). If the dielectric inhomogeneity occurs in a quadrant other than the fourth quadrant, then the simple permutation of the terms in (7.30) can be used to obtain the expression for φ_0 [1].

7.2.3 Neumann Boundary Condition and the Nodes on the Edge

Sometimes the normal derivative of the potential at the boundary is specified to determine the unique solution of the Laplace or Poisson equation. This condition is called the Neumann boundary condition. In this case, we may obtain the finite difference expression as follows.

Consider the geometry of Figure 7.8. In this case the potential at the central node is to be determined in terms of the potential at nodes 1, 2, 3, and the boundary condition about the line joining nodes 1 and 3. We know that if node 0 is the interior node, (7.11) can be used to determine φ_0 in terms of φ_1, φ_2, φ_3, and φ_4. However, node 4 condition is outside the solution domain and its value φ_4 is not known. This situation may occur if the nodes 0, 1, and 3 lie on an edge of the problem space. The outward normal derivative of potential at node 0, about the line joining the nodes 1 and 3, is expressed as

$$\frac{\partial\varphi}{\partial n} = \frac{\partial\varphi}{\partial y} = \frac{\varphi_2 - \varphi_4}{2\Delta y} \tag{7.31}$$

The value of φ_4 is thus obtained as

$$\varphi_4 = -2\Delta y \left.\frac{\partial\varphi}{\partial y}\right|_{\text{at the edge 31}} + \varphi_2 \tag{7.32}$$

Substituting for φ_4 in (7.11) gives

$$\varphi_0 \approx \frac{1}{4}\left(\varphi_1 + 2\varphi_2 + \varphi_3 - 2\Delta y \left.\frac{\partial\varphi}{\partial y}\right|_{\text{at the edge 31}}\right) \tag{7.33}$$

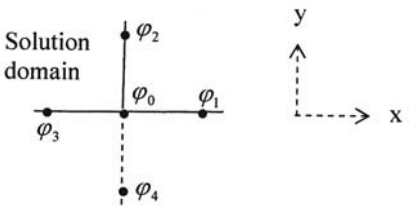

Figure 7.8 Node at an edge with the Neumann boundary condition specified normal to the edge 1–3.

A special but very common case is the *homogeneous* Neumann boundary condition $\partial\varphi/\partial n = 0$. It means $\varphi_2 = \varphi_4$ and the equipotential lines are perpendicular to the edge. For the Neumann boundary condition, (7.33) reduces to

$$\varphi_0 \approx \frac{1}{4}(\varphi_1 + 2\varphi_2 + \varphi_3) \tag{7.34}$$

Expression (7.34) applies to the nodes on the bottom edge of the problem space, with normal derivative zero at the edge. For the top edge, left-hand edge, and the right-hand edge, the corresponding expressions for φ_0 may be obtained by the simple permutation of (7.34) [1].

The homogeneous Neumann boundary condition may be used to reduce the size of the problems with magnetic wall or electric wall at the symmetry plane, for example, Example 7.1, shielded centered strip with two planes of symmetry (Problem 7.3), square coaxial line (Problem 7.4), double strip (Problem 7.5), and coaxial line with circular inner conductor (Problem 7.6).

Quiz 7.4. Consider the arrangement of nodes as shown in Figure 7.9. The expression for φ_5 subject to $\partial\varphi/\partial n = 0$ is given by ($\Delta x = \Delta y$):

(a) $\epsilon_0\varphi_5 = \frac{1}{4}(\epsilon_0\varphi_1 + (\epsilon_0 + \epsilon)\varphi_6 + \epsilon_0\varphi_9)$

(b) $\epsilon_0\varphi_5 = \frac{1}{4}(\epsilon_0\varphi_1 + 2\epsilon_0\varphi_6 + \epsilon_0\varphi_9)$

(c) $\epsilon_0\varphi_5 = \frac{1}{4}(\epsilon_0\varphi_1 + 2\epsilon\varphi_6 + \epsilon_0\varphi_9)$

Choose the correct expression and justify.

Answer. The expression (b) is correct, because similar to Figure 7.6 the contour is drawn enclosing node 5 and mid-way between node 5 and the surrounding nodes.

Quiz 7.5. For the arrangement of nodes shown in Figure 7.9 the expression for φ_6 is given by ($\Delta x = \Delta y$):

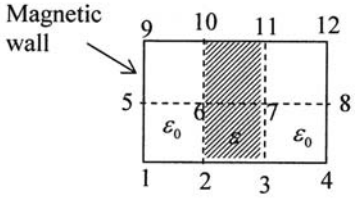

Figure 7.9 An arrangement of nodes for Quiz 7.4.

$$\text{(a)}\ \frac{\epsilon_0+\epsilon}{2}\varphi_6 = \frac{1}{4}\left(\epsilon_0\varphi_5 + \frac{\epsilon_0+\epsilon}{2}(\varphi_2+\varphi_7+\varphi_{10})\right)$$

$$\text{(b)}\ \frac{\epsilon_0+\epsilon}{2}\varphi_6 = \frac{1}{4}\left(\epsilon_0\varphi_5 + \frac{\epsilon_0+\epsilon}{2}(\varphi_2+\varphi_{10}) + \epsilon\varphi_7\right)$$

$$\text{(c)}\ \frac{\epsilon_0+\epsilon}{2}\varphi_6 = \frac{1}{4}\left(2\epsilon_0\varphi_5 + \frac{\epsilon_0+\epsilon}{2}(\varphi_2+\varphi_7+\varphi_{10})\right)$$

Choose the correct expression and justify.

Answer. The expression (b) is correct, because the contour is drawn enclosing node 6 and mid-way between node 6 and the surrounding nodes.

7.2.4 Node at a Corner

Consider the left-hand side bottom corner of the geometry shown in Figure 7.10. It consists of two intersecting edges and three nodes, 0, 1, and 2. The value φ_0 is to be determined in terms of φ_1, φ_2, and the normal derivatives $\partial\varphi/\partial x$ and $\partial\varphi/\partial y$ at the two edges of the corner. Proceeding in the same manner as in the last section, we can write

$$\varphi_4 = -2\Delta y \left.\frac{\partial\varphi}{\partial y}\right|_{\text{at the edge 01}} + \varphi_2 \tag{7.35a}$$

and

$$\varphi_3 = -2\Delta x \left.\frac{\partial\varphi}{\partial x}\right|_{\text{at the edge 02}} + \varphi_1 \tag{7.35b}$$

Use of (7.35) in (7.11) gives the following expression for φ_0:

$$\varphi_0 \approx \frac{1}{2}\left(\varphi_1 + \varphi_2 - \Delta y \left.\frac{\partial\varphi}{\partial y}\right|_{\text{at the edge 01}} - \Delta x \left.\frac{\partial\varphi}{\partial x}\right|_{\text{at the edge 02}}\right) \tag{7.36}$$

For the special case of homogeneous Neumann conditions $\partial\varphi/\partial x = \partial\varphi/\partial y = 0$, the above expression becomes

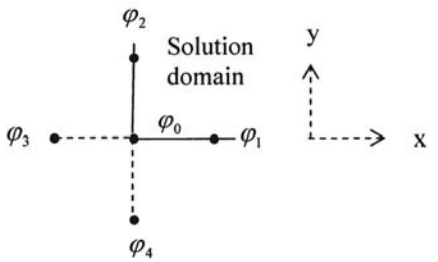

Figure 7.10 Node at a corner with the Neumann boundary conditions specified along two edges crossing at the corner.

$$\varphi_0 \approx \frac{1}{2}(\varphi_1 + \varphi_2) \tag{7.37}$$

The expressions for the potential at the nodes of right-hand bottom corner, left-hand top corner, and right-hand top corner can be written down by inspection of (7.37).

7.2.5 Node at an Edge with Dielectric Inhomogeneity About the Node

Consider the node at an edge with dielectric inhomogeneity about it as shown in Figure 7.11(a). The dielectric constant of the medium is ϵ in the second quadrant and ϵ_0 in the first quadrant. The edge condition is converted into symmetry condition about the x-axis by change in dielectric in the third quadrant as shown in Figure 7.11(b). The new geometry is similar to Figure 7.6. From (7.28) we can write

$$\varphi_0 \frac{\epsilon + \epsilon_0}{2} \approx \frac{1}{4}\left(\epsilon_0 \varphi_1 + \varphi_2 \frac{\epsilon + \epsilon_0}{2} + \epsilon\varphi_3 + \varphi_4 \frac{\epsilon + \epsilon_0}{2}\right) \tag{7.38}$$

Since $\partial/\partial y = 0$ means $\varphi_4 = \varphi_2$, the above expression becomes

$$\varphi_0(\epsilon + \epsilon_0) \approx \frac{1}{2}(\epsilon_0 \varphi_1 + \varphi_2(\epsilon + \epsilon_0) + \epsilon\varphi_3) \tag{7.39}$$

7.2.6 Treatment of Curved Boundaries

The finite difference method relies on a regular grid, which means only those geometries can be analyzed which can be fitted into regular grid patterns such as rectangular grid. In order to extend the validity of finite difference method to geometries with irregular shapes, some approximation in the contour of the given geometry or the modification of (7.11) for the nodes near the boundary may be

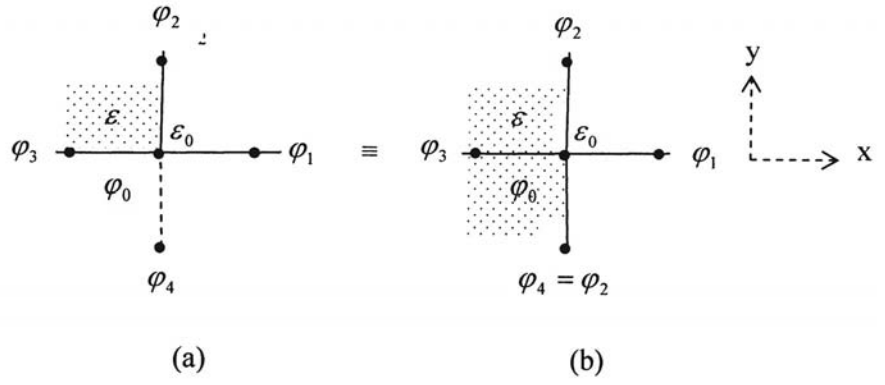

Figure 7.11 Neumann boundary condition with dielectric inhomogeneity about the central node: (a) original problem; and (b) equivalent problem.

attempted. The *stair-step* approximations to the curved boundary shown in Figure 7.12 may be attempted. The dotted curve *a* is the inside fit to the curved boundary, whereas curve *b* is the outside fit to the boundary. For better approximation, one can solve the problem twice for the dotted boundaries and take the average. Another approximation is the zigzag approximation through the curved boundary as shown in curve *c* of Figure 7.12. Modification of (7.11) for the nodes on the boundary is discussed next.

The nodes on an irregular boundary may be expressed as unequal separation between the nodes. Consider the irregular boundary and the finite difference nodes in Figure 7.13. The nodes 1 and 2 are on the boundary. Let the distance between the nodes 0 and 1 be $c_1 h$, and that between nodes 0 and 2 be $c_2 h$. Let us assume $c_3 = c_4 = 1$ to start with. The constants c_1 and c_2 lie between zero and one, and h is the normal spacing of the nodes. In this case, the potential φ_0 will be expressed in terms of φ_1, φ_2, φ_3, and φ_4.

Let us now assume that $\varphi(x)$ varies as a quadratic function of x in the vicinity of the boundary with [5]

$$\varphi(x) = \alpha_0 + \alpha_1 x + \alpha_2 x^2 \tag{7.40}$$

The constants α_0, α_1, and α_2 can be determined from the potential on three nodes along the x-direction. Using φ_0 at $x = 0$, φ_1 at $x = c_1 h$, and φ_3 at $x = -h$, we obtain

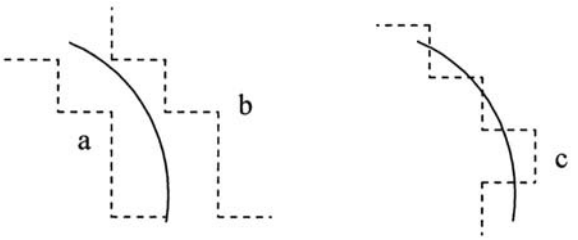

Figure 7.12 Stair-step approximations to the curved boundary in rectangular grid.

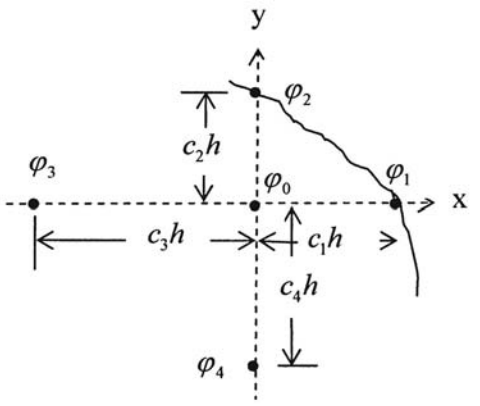

Figure 7.13 Curved boundary with nodes on it.

$$\varphi_0 = \alpha_0 \tag{7.41a}$$

$$\varphi_1 = \alpha_0 + \alpha_1 c_1 h + \alpha_2 c_1^2 h^2 \tag{7.41b}$$

$$\varphi_3 = \alpha_0 - \alpha_1 h + \alpha_2 h^2 \tag{7.41c}$$

Solution of these equations for α_2 yields

$$\alpha_2 = \frac{\varphi_1 - (1 + c_1)\varphi_0 + c_1 \varphi_3}{c_1 h^2 (1 + c_1)} \tag{7.42}$$

Taking the double derivative of (7.40) gives

$$\frac{\partial^2 \varphi}{\partial x^2} = 2\alpha_2 \tag{7.43}$$

Therefore,

$$\frac{\partial^2 \varphi}{\partial x^2} = 2\,\frac{\varphi_1 - (1 + c_1)\varphi_0 + c_1 \varphi_3}{c_1 h^2 + c_1^2 h^2} \tag{7.44}$$

This expression reduces to the standard finite difference form for $c_1 = 1$. Similarly,

$$\frac{\partial^2 \varphi}{\partial y^2} = 2\,\frac{\varphi_2 - (1 + c_2)\varphi_0 + c_2 \varphi_4}{c_2 h^2 + c_2^2 h^2} \tag{7.45}$$

Adding (7.44) and (7.45) and applying the Laplace equation gives

$$\varphi_0 \left[\frac{1}{c_1} + \frac{1}{c_2}\right] = h^2 \frac{\varphi_1 + c_1 \varphi_3}{c_1 h^2 (1 + c_1)} + \frac{\varphi_2 + c_2 \varphi_4}{c_2 h^2 (1 + c_2)} \tag{7.46}$$

Expression (7.46) should be used in place of (7.11) for nodes near the irregular boundary. It reduces to (7.11) for $c_1 = c_2 = 1$.

The above procedure may be generalized for an arbitrary separation between the nodes as shown in Figure 7.13

$$\varphi_0 \left[\frac{1}{c_1 c_3} + \frac{1}{c_2 c_4}\right] = \left[\frac{c_3 \varphi_1 + c_1 \varphi_3}{c_1 c_3 (c_1 + c_3)} + \frac{c_4 \varphi_2 + c_2 \varphi_4}{c_2 c_4 (c_2 + c_4)}\right] \tag{7.47}$$

One of the attractive features of the finite difference method is the conversion of the differential form of the equation to the algebraic form like (7.12). If the parameters of the problem are chosen judiciously, coarse discretization and symmetry properties may be used to reduce the number of simultaneous equations. Analytical

solutions of these equations may be attempted to obtain design guidelines. This step may be followed by accurate analysis with finer discretization. An example is attempted next and in Section 7.3.4 to describe the procedure.

7.2.7 Finite Difference Analysis of an Inhomogeneously Filled Parallel Plate Capacitor

As an application of interface and Neumann boundary conditions, let us analyze the parallel plate capacitor of Figure 7.14 using FDM. The upper plate is charged to 1 volt and the lower plate is grounded. The side walls are terminated in magnetic wall boundary condition to limit the size of the problem in FDM. This amounts to neglecting the fringing fields of the capacitor. Analytical solution for this geometry is available [8, p. 124] with which we can compare the FDM solution.

For FDM analysis, the capacitor geometry is discretized into square cells with $\Delta x = \Delta y = a$. The boundary conditions at the top and bottom plates lead to $\varphi_9 = \varphi_{10} = \varphi_{11} = \varphi_{12} = 1\text{V}$; $\varphi_1 = \varphi_2 = \varphi_3 = \varphi_4 = 0$. The unknown potentials are then φ_5, φ_6, φ_7, and φ_8. From the symmetry of the structure about the y-axis we can write $\varphi_5 = \varphi_8$ and $\varphi_6 = \varphi_7$.

We now use the interface condition of Section 7.2.1 and Neumann boundary condition of Section 7.2.3 to write the following expressions for the potentials at nodes 6 and 5:

$$\frac{\epsilon_0 + \epsilon}{2}\varphi_6 = \frac{1}{4}\left(\frac{\epsilon_0 + \epsilon}{2}\varphi_5 + \frac{\epsilon_0 + \epsilon}{2}\varphi_7 + \epsilon_0\varphi_{10} + \epsilon\varphi_2\right) \tag{7.48}$$

$$\frac{\epsilon_0 + \epsilon}{2}\varphi_5 = \frac{1}{4}\left(\epsilon\varphi_1 + 2\frac{\epsilon_0 + \epsilon}{2}\varphi_6 + \epsilon_0\varphi_9\right) \tag{7.49}$$

Applying the boundary and symmetry conditions leads to the following solution:

$$\varphi_5 = \varphi_6 = \frac{\epsilon_0}{\epsilon_0 + \epsilon} = \varphi_7 = \varphi_8 \tag{7.50}$$

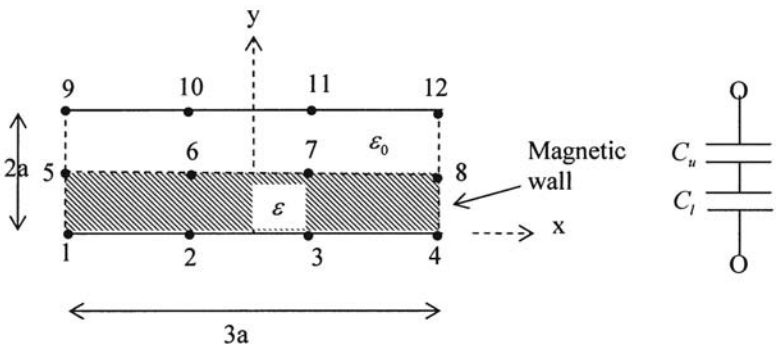

Figure 7.14 An inhomogeneously filled parallel plate capacitor and its equivalent circuit.

In order to determine the capacitance per unit length C_0, we calculate the energy stored in the electric field as

$$W_e = \frac{1}{2}\iint \epsilon |\nabla\varphi|^2 \, ds = \frac{1}{2}\iint \epsilon |\mathbf{E}|^2 \, ds \tag{7.51}$$

where the integration is carried out over the cross-section of the capacitor. The electric field intensity is given by

$$E_y(y) = -\left(\frac{\varphi(y + \Delta y) - \varphi(y)}{\Delta y}\right) \text{ V/m} \tag{7.52}$$

For the region between the top plate and the interface, the electric field is constant and is given by

$$E_y = -\left(\frac{\varphi_9 - \varphi_5}{a}\right) \text{ V/m} = -\left(\frac{\epsilon}{a(\epsilon_0 + \epsilon)}\right) \text{ V/m} \tag{7.53}$$

The energy stored in this region is therefore obtained as

$$W_e^{\epsilon_0} = \frac{1}{2}\epsilon_0 \int_{a}^{2a}\int_{-3a/2}^{3a/2} \left(\frac{\epsilon}{a(\epsilon + \epsilon_0)}\right)^2 dx\,dy = \frac{3}{2}\epsilon_0 \left(\frac{\epsilon}{\epsilon + \epsilon_0}\right)^2 \tag{7.54a}$$

The energy stored in the lower half of the capacitor is similarly given by

$$W_e^{\epsilon} = \frac{1}{2}\epsilon \int_{0}^{a}\int_{-3a/2}^{3a/2} \left(\frac{\epsilon_0}{a(\epsilon + \epsilon_0)}\right)^2 dx\,dy = \frac{3}{2}\epsilon \left(\frac{\epsilon_0}{\epsilon + \epsilon_0}\right)^2 \tag{7.54b}$$

The total energy stored in the capacitor is therefore

$$W_e = W_e^{\epsilon_0} + W_e^{\epsilon} = \frac{3}{2}\frac{\epsilon\epsilon_0}{\epsilon + \epsilon_0} \tag{7.55}$$

Equating W_e to $\frac{1}{2}C_0 V^2$, where V is the potential difference between the plates ($V = 1$ volt), yields the following expression for capacitance:

$$C_0 = \frac{3\epsilon\epsilon_0}{\epsilon + \epsilon_0} \tag{7.56}$$

The analytical expression for the capacitance may be obtained by modeling the parallel plate geometry as a series combination of capacitors due to the upper half and lower half portions, as shown in Figure 7.14 [8]. The capacitance of the upper

half portion is given by $C_u = 3\epsilon_0$, whereas $C_l = 3\epsilon$ for the lower half geometry. Series combination of C_u and C_l results in C_0, the FDM expression derived above.

It may be observed from the above analysis that in spite of crude discretization used here, the FDM result matches exactly with the analytical expression; that is, the discretization error is zero in this case. The reason for this accuracy lies in the potential distribution we are modeling using FDM. The expected potential distribution is linearly varying along the y-direction and is constant along the x-direction.

7.3 Finite Difference Analysis of Guiding Structures

The method of finite differences has been used successfully to solve many diverse problems [7, 10, 11] including transmission lines [12–15], waveguides [16–19], and microwave circuits [20–22]. Finite difference analysis of microstrip line, rectangular waveguide, and ridge waveguide is discussed next. The effect of discretization error on the propagation constant leading to numerical dispersion is also included.

7.3.1 Analysis of Enclosed Microstrip Line

Consider the cross-section of a microstrip line as shown in Figure 7.15. It consists of a metal strip of width W on a grounded dielectric substrate of thickness d and dielectric constant ϵ_1. The free space above the strip and the dielectric substrate are infinite in size. The open region geometry gives rise to an infinite number of nodes, which is impossible to solve on computers due to limited computer resources. The metal enclosure around the microstrip line has been placed here to limit the number of nodes. The characteristics of the line remain unaffected if the enclosure size is sufficiently large.

The characteristic impedance and the phase velocity of the transmission line can be determined from the capacitance per unit length of the line as described in Section 1.14.

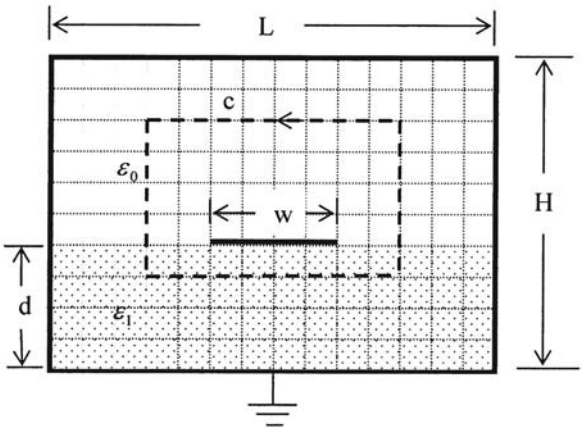

Figure 7.15 Cross-section of an enclosed microstrip line.

The potential distribution in the microstrip line is determined by discretizing the geometry and satisfying the Laplace equation at the free nodes, as described in Example 7.1. The only difference is that the nodes at the interface are subjected to (7.28) and not (7.12). Once the potential distribution has been obtained, the charge on the strip may be obtained using Gauss law, described as

$$\oiint_s \epsilon \mathbf{E}.\mathbf{ds} = q \tag{7.57a}$$

Since the cross-section of the microstrip line does not change along its length, the charge distribution on the strip also remains same with length. Integrating over unit length gives

$$\oint_c \epsilon \mathbf{E}.\mathbf{dc} = q_l$$

where q_l is the charge per unit length, and c is the contour enclosing the strip. The above expression may be written as

$$-\oint_c \epsilon \nabla\varphi.\mathbf{dc} = q_l, \qquad \text{since } \mathbf{E} = -\nabla\varphi$$

or

$$\oint_c \epsilon \frac{\partial\varphi}{\partial n} dc = -q_l \qquad \text{C/m} \tag{7.57b}$$

The charge density q_l can be determined by utilizing the nodal potential values about the contour. The contour c for computing the charge enclosed is shown separately in Figure 7.16. The contour integration is carried out here in the form of summation by dividing the contour in smaller segments. Applying the definition of $\partial\varphi/\partial n$ along this contour, we obtain [2]

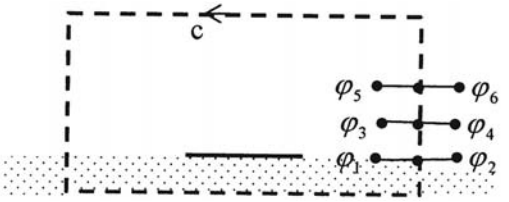

Figure 7.16 Contour c and the nodes employed in calculating the charge.

$$\ldots + \epsilon_0 \left(\frac{\varphi_6 - \varphi_5}{2h}\right) h + \epsilon_0 \left(\frac{\varphi_4 - \varphi_3}{2h}\right) h + \epsilon_0 \left(\frac{\varphi_2 - \varphi_1}{2h}\right) \frac{h}{2} + \epsilon_1 \left(\frac{\varphi_2 - \varphi_1}{2h}\right) \frac{h}{2} + \ldots$$

$$+ \text{contribution from other sides of the contour} = q_l \tag{7.58}$$

Here h is the separation between the nodes in either direction.

The line capacitance is given by

$$C_0 = \frac{q_l}{V} \tag{7.59}$$

where V is the assumed potential difference between the strip and the ground plane, normally 1 volt.

The microstrip line is next completely filled with air and the above procedure is repeated to calculate C_0^a, the capacitance per unit length with air as dielectric. These values of capacitances are used to determine the characteristic impedance Z_0 and the effective dielectric constant ϵ_{re} according to (1.62). A Fortran source code for the finite difference analysis of microstrip line is included in [4].

In order to compare the results with the data reported in [2], we select the following parameters (in arbitrary units) for the microstrip line of Figure 7.15:

$$H = 2,\ L = 7.0,\ d = 1.0,\ W = 1.0,\ \epsilon_1 = 9.6\epsilon_0$$

The dimensions are normalized to d. The actual dimensions, whether expressed in meters or microns or any other unit, is not important here.

There are a number of issues to be discussed before we present the final results. These are related to the convergence aspect of the FDM, the number of cells per unit length N, the number of iterations I used for solving the set of simultaneous equations iteratively, and accuracy of results.

Convergence

All the computations reported here are carried out using the source code *mstrip.m*. Figure 7.17 shows the effect of number of nodes or node density on the characteristic impedance of microstrip line. It may be noted that the impedance value converges for $N \geq 24$. The number of iterations used for each point of calculation is 1,000 because SOR is not used here. A large number of nodes on the strip are required for accurate calculation of Z_0. This is related to the physical charge density distribution on the strip. Due to the mutual repulsion between free charges on the strip, the charge density should be large at the ends and flat in the middle for a zero thickness strip. The charge density is plotted in Figure 7.18 for two different values of N. It is seen that $N = 24$ gives rise to a larger peak/minimum value of charge density compared to $N = 20$ case, and therefore more accurate value of Z_0.

We next discuss the optimum number of iterations, I. The value of Z_0 is expected to be sensitive to I because the calculation of charge on the strip involves derivative of potential, (7.58). *A sufficiently large number of iterations will produce an accurate potential distribution about the strip from which we can determine an*

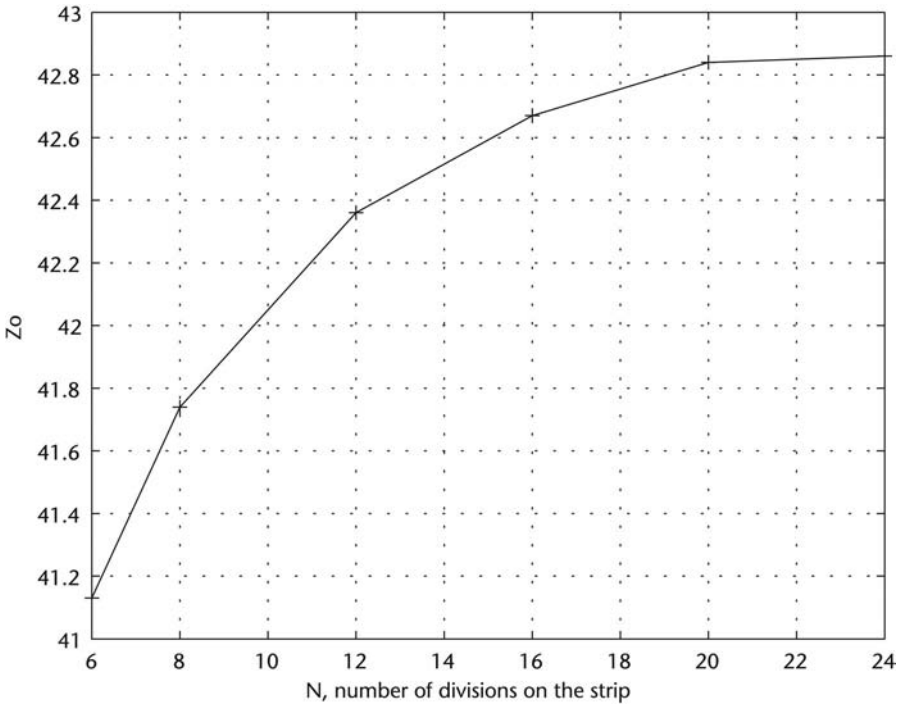

Figure 7.17 Computed characteristic impedance of the microstrip line as a function of node density N. $W/d = 1$, $\epsilon_r = 9.6$, $I = 1{,}000$.

accurate value of $\partial\varphi/\partial n$. Variation of Z_0 as a function of number of iterations I is plotted in Figure 7.19 for $N = 20$. The converged value of I is 2,000. The equipotential contours about the strip are plotted in Figure 7.20. For this we have used the MATLAB command *contour*. This plot may be used for the diagnostics of the data generated. It may be noted that the equipotential contours are similar to the magnetic field lines encircling the strip. Finally, the electric field distribution about the strip is plotted in Figure 7.21. The electric field is not tangential to the interface because of refraction there.

The computed characteristic impedance and the effective dielectric constant for the microstrip line are given in Table 7.1 for various values of W/d. The value of I used is 1,800 and $N = 24$. For comparison, the impedance reported in [2] for $W/d = 1$ is 42.76 ohms. It may be noted from Table 7.1 that the effective dielectric constant ϵ_{re} for the given geometry is nearly equal to $(\epsilon_r + 1)/2$. This is because the microstrip line behaves like a strip line for $H = 2d$. The characteristic impedance Z_0 of strip line is given by (11.115) with ϵ_r replaced by $(\epsilon_r + 1)/2$. The exact value for strip line for $W/d = 1$, $\epsilon_r = 9.6$, $b = 2d$ is 43.65 ohms, which is very close to the finite difference value of 42.98 ohms. The error in the computed value based on FDM is due to the discretization of microstrip line.

This code *mstrip.m* may also be employed to analyze a shielded strip line by homogeneous filling of the enclosed microstrip configuration. Use of SOR reduced the number of iterations from 2,000 to 250. Square grid with the value of omega, given by (7.22b), was used for the purpose.

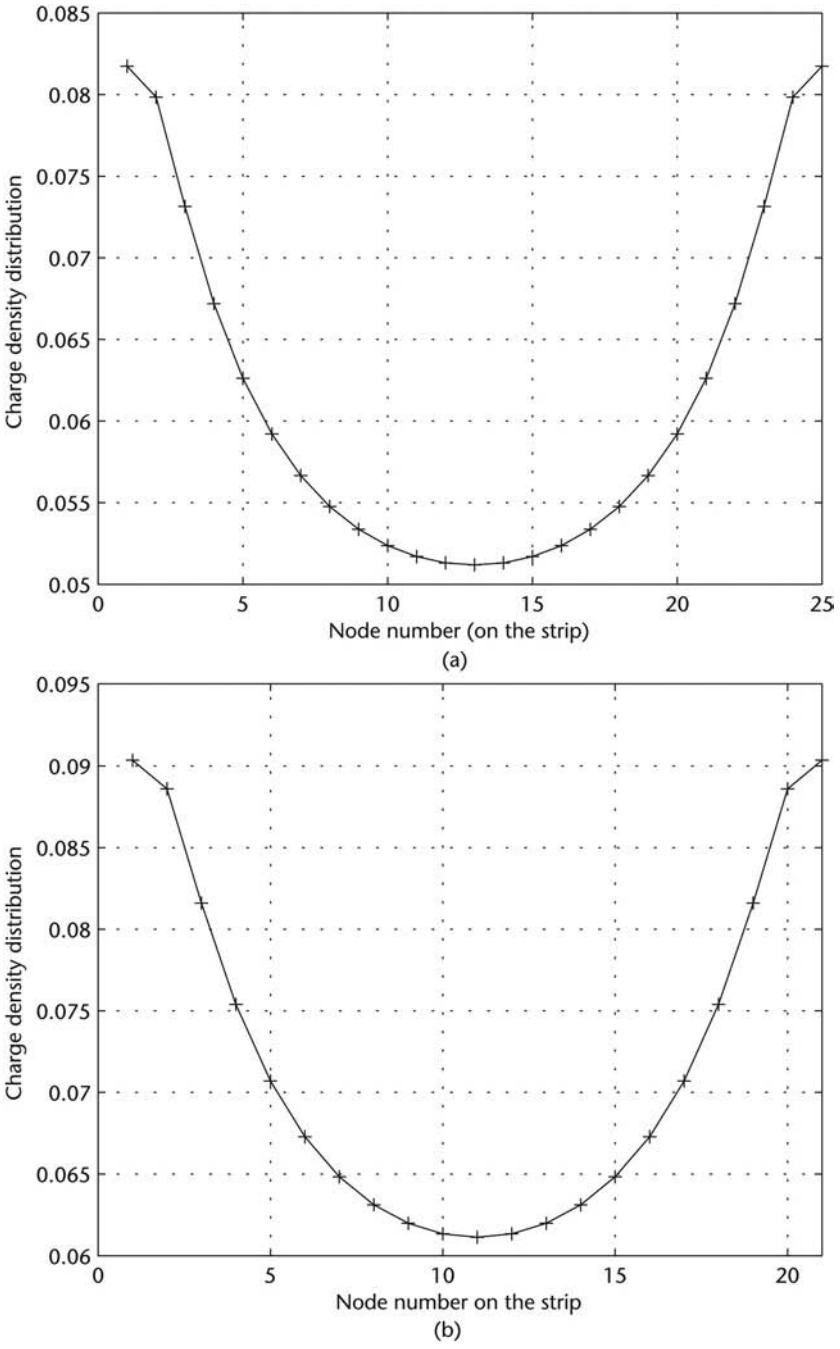

Figure 7.18 Charge density distribution on the strip for $W/d = 1$, $\epsilon_r = 9.6$: (a) $N = 24$, $I = 2{,}000$; and (b) $N = 20$, $I = 2{,}000$.

Effect of Strip Thickness

It has been assumed in the analysis described above that the metal strip thickness is zero. The effect of strip thickness on the line impedance can be included in the FDM analysis easily. For this, the discretization of the line geometry is carried out

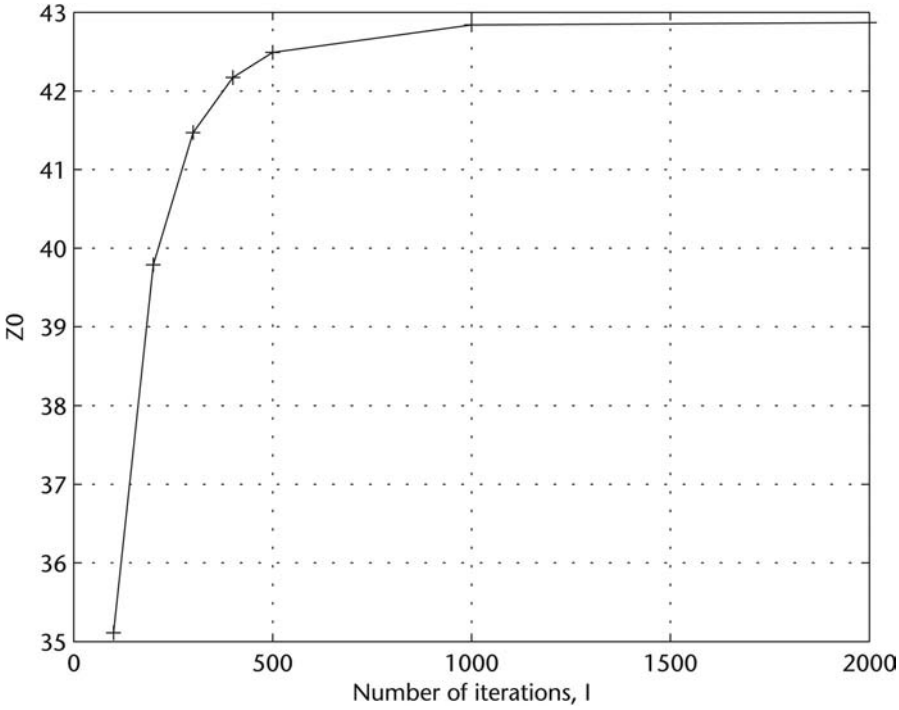

Figure 7.19 Variation of W/d of microstrip as a function of number of iterations I. $W/d = 1$, $\epsilon_r = 9.6$, $N = 20$.

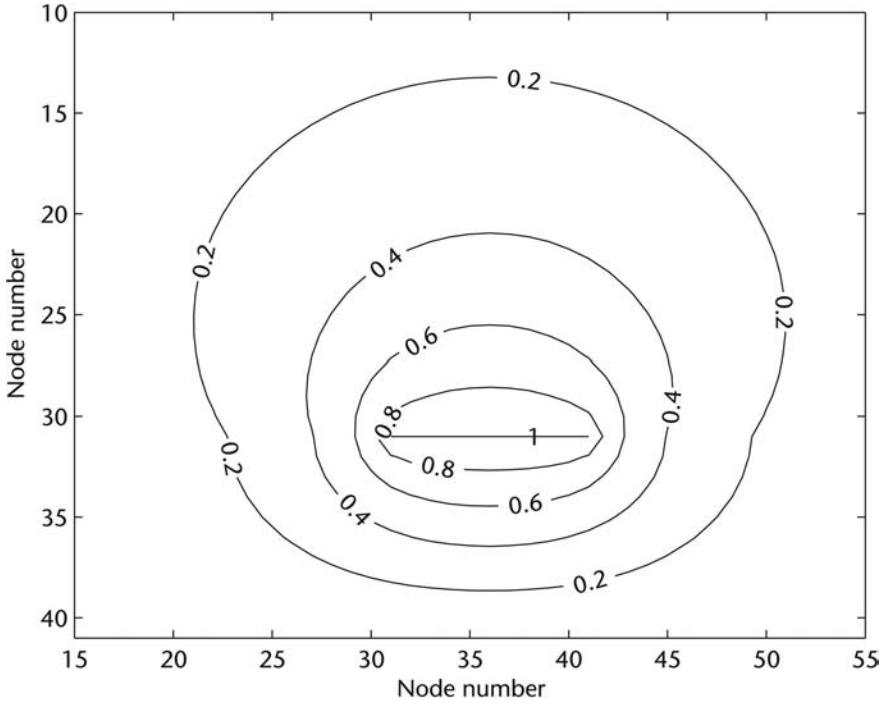

Figure 7.20 Equipotential contours about the strip, $V = 1$ at the strip. $N = 10$, $I = 1{,}000$, $W/d = 1$, $H/d = 5$, $L/d = 7$, $\epsilon_r = 9.6$.

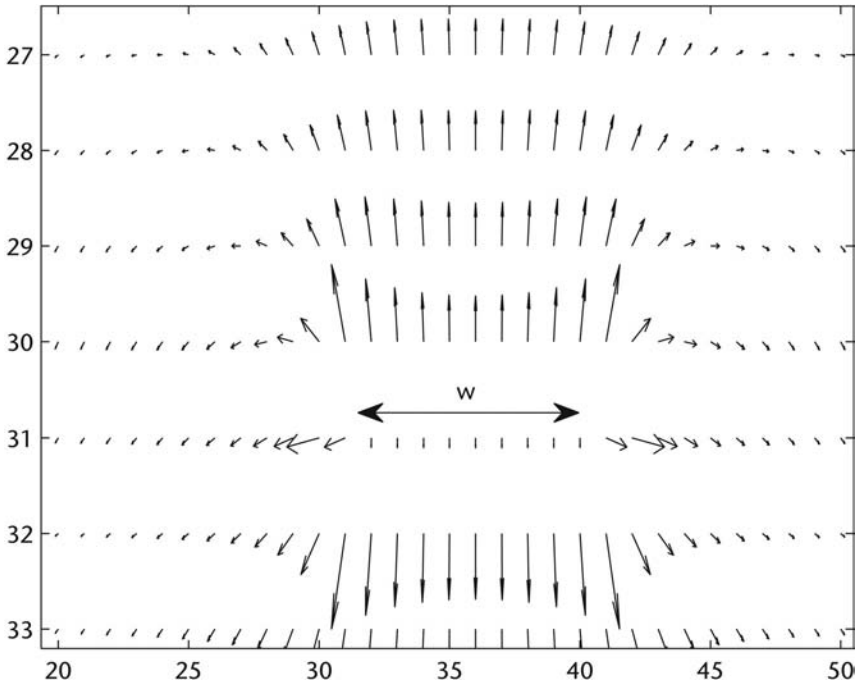

Figure 7.21 Electric field distribution about the strip, $V = 1$ at the strip. $N = 10$, $I = 1{,}000$, $W/d = 1$, $H/d = 5$, $L/d = 7$, $\epsilon_r = 9.6$.

Table 7.1 Computed FDM Results for a Microstrip Line with $H = 2$, $L = 7$, $\epsilon_r = 9.6$

Characteristic → W/d ↓	Z_0	ϵ_{re}
1	42.98	5.297
1.5	33.97	5.299
2	28.11	5.299
2.5	23.98	5.299

as before and all the nodes on the strip are assigned the same potential, 1 volt in the present case. The discretized strip with strip thickness $t = \Delta y$ is shown in Figure 7.22. The Gaussian contour c, for the determination of q_l, may have to be redrawn so that it encloses the strip.

Nonuniform Discretization

It may be observed from Figure 7.18 that the charge density on a metal strip is maximum at the edges and minimum at the center. This distribution can be modeled

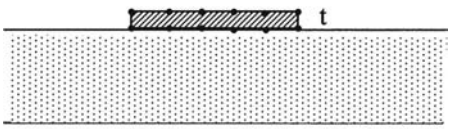

Figure 7.22 Discretization of metal strip for nonzero value of strip thickness t, $\Delta x = 2\Delta y$.

more efficiently if we discretize the strip nonuniformly; that is, the step size h should be smaller near the edges and larger in the middle. One may use the following expression to describe the coordinates of nodes on a strip of width W:

$$x_i = -\frac{W}{2}\cos\frac{i\pi}{N}, \qquad i = 1, 2, 3, \ldots N \qquad \text{for } -\frac{W}{2} < x < \frac{W}{2} \tag{7.60}$$

7.3.2 Analysis of Geometries with Open Boundaries

In the finite difference analysis in the last section, we enclosed the microstrip line in a metal box to limit the number of nodes for the open region problem. But, we do not know the appropriate size of the box. For this one may carry out a number of simulations for increasing the size of the box. The resulting data for Z_0 may be used to plot a curve as a function of box size. This curve can be extrapolated to determine the value of Z_0 for an open region problem. The accuracy of the solution depends on the size of the box used to enclose the device. An alternative approach for the open boundary problems is to use a fictitious boundary [23] outside the device, or the use of asymptotic boundary conditions [24]. The first method is an iterative method in which the approximate potential distribution inside the fictitious boundary is used to calculate the total charge enclosed. This charge distribution is next used to determine the potential on the boundary. This procedure is repeated iteratively to produce the correct potential distribution on the fictitious boundary. For a microstrip line geometry, the results at the interior nodes are found to be independent of the location of the boundary for a grid size larger than 18×12 [23].

The asymptotic boundary condition (ABC) is a (local) radiation boundary condition expressed as a partial differential equation. The enclosure of Figure 7.15 at which $\varphi = 0$ has been assumed, may be called the 0th order ABC. The first order ABC at the x = constant boundary is defined as

$$\left.\frac{\partial\varphi}{\partial x}\right|_{boundary} = -\frac{1}{x}\left(\varphi + y\left.\frac{\partial\varphi}{\partial y}\right|_{boundary}\right) \tag{7.61}$$

Similarly, the ABC at the other boundaries can be written down. Second order ABC is also described in [24]. The partial derivatives in (7.61) can be described in terms of the nodal values near the boundary, which are already known. The use of first-order and second-order ABC may be used to bring the boundary close to the device without affecting the device characteristics. This reduces the size of the matrix to be solved. However, the number of iterations required (if iterative method is used) to determine the nodal values increase considerably compared to the 0th order ABC, because the nodal values at the boundaries are not fixed and depend on the value at neighboring nodes and change with iteration.

Another approach for analyzing open boundary problems is to combine conformal mapping and FDM for problems in electrostatics. Conformal mapping may be used to reduce the open region problems like that of planar lines to closed geometry (Chapter 4). FDM may now be used to determine the capacitance of this geometry [25].

Effect of the discretization error on dispersion is discussed next.

7.3.3 Wave Propagation and Numerical Dispersion

We have discussed the error associated with the discretization of function and by implication the discretization of domain in Section 6.3. The discretization is necessary so that computers may be used to solve problems with arbitrary shape and dielectric inhomogeneity. When FDM is used to solve problems based on wave propagation, we come across a phenomenon called numerical dispersion. In this case the wave suffers dispersion, and the propagation constant becomes a function of frequency, even though the medium may be dispersionless. To describe this behavior mathematically we consider the solution of one-dimensional scalar Helmholtz equation [26],

$$\frac{d^2E_y}{dz^2} + k_0^2 E_y(z) = 0 \tag{7.62}$$

The traveling wave solution of this wave equation is of the form

$$E_y(z) = E_0 e^{\pm jk_0 z} \tag{7.63}$$

Let us now discretize (7.62), determine the propagation constant, and compare it with k_0 to determine the numerical dispersion.

We assume a large free space with no boundaries and discretize it uniformly with cell size Δz, as shown in Figure 7.23. The central difference approximation of the double derivative in (7.62) gives rise to the following form of discretized Helmholtz equation about node i:

$$2E_y(i) - E_y(i-1) - E_y(i+1) - (k_0\Delta z)^2 E_y(i) = 0 \tag{7.64}$$

We now solve this equation using a discretized version of (7.63); that is,

$$E_y(i) = E_0 e^{\pm j\beta(i\Delta z)} \tag{7.65}$$

where β is the propagation constant in the discretized medium. Substituting the proposed solution in (7.64) gives

$$(2 - (k_0\Delta z)^2)E_0 - E_0 e^{j\beta\Delta z} - E_0 e^{-j\beta\Delta z} = 0$$

or

$$2 - (k_0\Delta z)^2 = 2\cos(\beta\Delta z) \tag{7.66a}$$

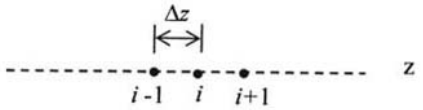

Figure 7.23 Discretized one-dimensional space for wave propagation.

or

$$\beta = \frac{1}{\Delta z} \cos^{-1}\left(1 - \frac{(k_0 \Delta z)^2}{2}\right) \tag{7.66b}$$

Equations (7.65) and (7.66b) constitute the numerical solution for wave propagation on an infinite, uniform mesh. The propagation constant β is found to be different from the free space propagation constant k_0 and is dependent on cell size Δz and k_0. In the limiting case, $\Delta z \to 0$, $\beta \to k_0$ as expected. In the lossless medium, β is real valued for $\cos(\beta \Delta z) \geq -1$ or

$$k_0 \Delta z \leq 2 \tag{7.67}$$

Therefore, for cell sizes smaller than $\Delta z \cong \lambda_0/\pi$, *the error in the numerical solution is simply phase error*. The phase error across a single cell is given by

$$\text{Phase error} = (k_0 - \beta)\Delta z \tag{7.68}$$

The phase error per wavelength is listed in Table 7.2 as a function of $\Delta z/\lambda_0$. It is observed from this table that $\beta > k_0$ for all values of cell size. Also, the phase error decreases as h^2. For example, the phase error per λ_0 is –6.19° for $\Delta z = \lambda_0/10$ and decreases to almost one-fourth of this value when the cell size is made half. The error is less than 1% for $\Delta z/\lambda_0 < 0.055$.

Exercise. Determine the rate of covergence and the extrapolated value for β/k_0 from the data given in Table 7.2.

Quiz 7.6. Table 7.2 shows that $\beta/k_0 > 1$ for the discretizations employed. The effective relative dielectric constant ϵ_{re} of the medium, defined as $\epsilon_e = \epsilon_0 \epsilon_{re}$ (similar to that for a microstrip line), is given by

(a) $\epsilon_{re} < 1$;
(b) $\epsilon_{re} > 1$;
(c) $\epsilon_{re} = 1$;
(d) none of the above.

Choose the correct option and explain why.

Answer. (b).

Table 7.2 Phase Constant and Phase Error per Wavelength as a Function of Cell Size $\Delta z/\lambda_0$

$\Delta z/\lambda_0$	$\beta \Delta z$ (*rad*)	$k_0 \Delta z$ (*rad*)	*Phase Error per* λ_0 (*deg*)
1/4	1.8067	1.5708	–54.06°
1/5	1.3588	1.2566	–29.27°
1/10	0.6391	0.6283	–6.19°
1/20	0.31546	0.31416	–1.49°

7.3.4 Analysis of Ridge Waveguide

Next we apply the finite difference method to the eigenvalue problem in rectangular waveguides, Figure 7.24. The governing PDE in this case is the Helmholtz or wave equation

$$\nabla^2 \varphi + k^2 \varphi = 0 \tag{7.69}$$

where $\varphi = E_z$ for the *TM* modes, or H_z for the *TE* modes, and $k = \omega\sqrt{\mu\epsilon}$ is the wave number. The permittivity ϵ and permeability μ characterize the medium filling the waveguide. They may be real for lossless medium and complex for lossy medium. The variation of fields along the longitudinal direction is assumed to be $\exp(j\beta z)$, and the wave equation reduces to the two-dimensional form as

$$\frac{\partial^2 \varphi}{\partial x^2} + \frac{\partial^2 \varphi}{\partial y^2} + k_c^2 \varphi = 0 \tag{7.70}$$

where

$$k_c^2 = k^2 - \beta^2 \tag{7.71}$$

and is called the cutoff wavenumber. In the eigenvalue problem (7.70), the unknowns are k_c and φ. For each eigenvalue k_i there is a corresponding eigenfunction φ_i, which represents the field configuration of a propagating mode.

Now we discretize the waveguide using a square mesh as shown in Figure 7.24, and apply the FDM. Use of (7.15) for square grid in (7.70) gives

$$\varphi(i+1, j) + \varphi(i-1, j) + \varphi(i, j-1) + \varphi(i, j+1) - \left(4 - h^2 k_c^2\right)\varphi(i, j) = 0 \tag{7.72}$$

where $h = \Delta x = \Delta y$ is the mesh size. Equation (7.72) is applied to the all the free nodes. For the nodes on the boundary of the waveguide, Dirichlet condition

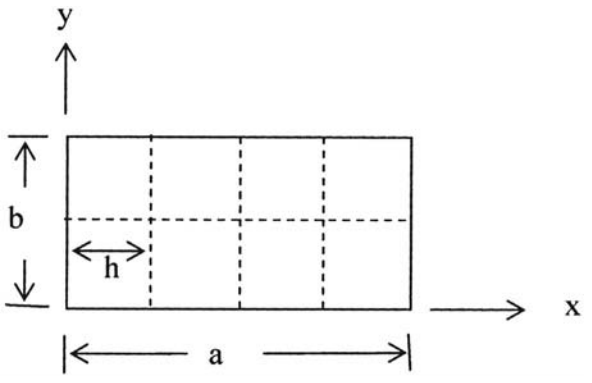

Figure 7.24 Rectangular waveguide discretized in square cells for analysis using FDM ($a = 2b$).

($\varphi = 0$) is applicable for the *TM* modes, and Neumann condition ($\partial\varphi/\partial n = 0$) for the *TE* modes. The Neumann condition is specified by (7.34). By applying (7.72) to all the nodes in the cross-section of the waveguide, we obtain a set of simultaneous equations which can be cast into the matrix equation

$$([A] - \lambda[I])[\varphi] = [0] \qquad \text{or} \qquad [A][\varphi] = \lambda[\varphi] \tag{7.73}$$

where A is the coefficient matrix of known integer elements, and

$$\lambda = 4 - h^2 k_c^2 \tag{7.74}$$

is the unknown eigenvalue, I is an identity matrix, and $\varphi = (\varphi_1, \varphi_2, \varphi_3, \ldots)$ is the eigenvector. The set of simultaneous equations represented by (7.73) will have nonzero solution only if the determinant of the matrix vanishes; that is,

$$\det[A - \lambda I] = 0 \tag{7.75}$$

There are several ways of determining λs and the corresponding eigenfunctions φs. We describe two approaches here [2, 4].

Direct Solution Method

In this method, $\det[A - \lambda I]$ is set equal to zero, and results in a polynomial in λ which can be solved for the various eigenvalues λs. For each of these eigenvalues the corresponding eigenfunction φ is obtained from the matrix equation $A\varphi = \lambda\varphi$. This method requires storing the matrix elements and is therefore used for small sized matrices.

Example 7.2. Let us determine the cutoff frequency of modes in a rectangular waveguide. The dimensions of the waveguide and discretization are selected such that it produces a small sized matrix which can be solved almost analytically. In the process we will clarify some of the computational aspects. The rectangular waveguide is analyzed for the *TE* mode cut off.

As shown in Figure 7.25(a), the waveguide with aspect ratio 2:1 is discretized in square cells of size $h \times h$. The total number of nodes is 15 and all of these are free nodes for the *TE* modes. In order to keep the matrix size small, we shall assume TE_{n0} modes for analysis. For constant field distribution E_y along the height of the waveguide, the potential φ is also constant along the height; that is,

$$\varphi_{11} = \varphi_6 = \varphi_1 \qquad \varphi_{12} = \varphi_7 = \varphi_2 \qquad \varphi_{13} = \varphi_8 = \varphi_3 \tag{7.76}$$

and so on. Therefore, we need to determine the potential at nodes 1, 2, 3, 4, and 5 only. The problem therefore becomes one-dimensional. The size of the problem can be reduced further if we restrict the solutions for n = odd or even modes only. For odd modes, the potential function $\varphi = H_z$ is odd symmetric about the plane passing through 13-3-8 and maximum at the side walls. Therefore, the device geometry reduces to that shown in Figure 7.25(b) with $\varphi_3 = 0$. Applying (7.72) for the potential at the nodes 1 and 2 gives

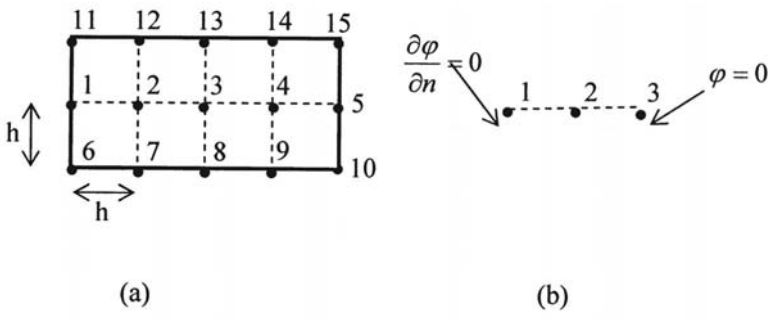

Figure 7.25 Simplification of the analysis of a rectangular waveguide using symmetry. (a) Discretized geometry before symmetry consideration. (b) Waveguide geometry for the analysis of TE_{n0} (n, odd) modes. Odd symmetry about 13-3-8 plane results in $\varphi = 0$ at this plane.

$$\lambda\varphi_1 = \varphi_{11} + 2\varphi_2 + \varphi_6 \qquad \text{using (7.34) for the edge condition} \tag{7.77}$$

$$\lambda\varphi_2 = \varphi_1 + \varphi_{12} + \varphi_3 + \varphi_7 \tag{7.78}$$

where λ has been defined in (7.74). Use of (7.76) and $\varphi_3 = 0$ gives

$$(\lambda - 2)\,\varphi_1 = 2\varphi_2 \qquad \text{and} \qquad (\lambda - 2)\,\varphi_2 = \varphi_1 \tag{7.79}$$

or

$$\begin{bmatrix} \lambda - 2 & -2 \\ -1 & \lambda - 2 \end{bmatrix} \begin{bmatrix} \varphi_1 \\ \varphi_2 \end{bmatrix} = 0 \tag{7.80}$$

The eigenvalue equation is obtained by setting the determinant to zero. We obtain $(\lambda - 2)^2 = 2$, and the eigenvalues are $\lambda_1 = 2 + \sqrt{2}$ and $\lambda_2 = 2 - \sqrt{2}$. The corresponding values of k_c obtained from (7.74) are $h^2 k_{c1}^2 = 2 - \sqrt{2}$ and $h^2 k_{c2}^2 = 2 + \sqrt{2}$. The first eigenvalue gives

$$\left(\frac{2\pi h}{\lambda_{c1}}\right)^2 = 2 - \sqrt{2}, \qquad k_c = \frac{2\pi}{\lambda_c}$$

or

$$\lambda_{c1} = \frac{2\pi h}{\sqrt{0.586}} \tag{7.81}$$

For $h = a/4$, where a is the width of the waveguide, one obtains

$$\lambda_{c1} = \frac{\pi a}{2\sqrt{0.586}} = 2.05a \tag{7.82}$$

This value is very close to the exact value of $2a$ for the TE_{10} mode. The eigenfunction for the mode is obtained by substituting $\lambda = \lambda_1 = 2 + \sqrt{2}$ in (7.80) and solving for φ_1 and φ_2. It yields, $\varphi_2 = \varphi_1/\sqrt{2}$, which is exactly the value obtained from $\cos(\pi x/a)$.

The second eigenvalue $\lambda_2 = 2 - \sqrt{2}$ leads to

$$\lambda_{c2} = \frac{\pi a}{2\sqrt{3.414}} = 0.849a \tag{7.83}$$

The exact cutoff wavelength for the TE_{30} mode is $0.667a$.

Iterative Solution Method

In this method, we begin with the assumed values of φ_1, φ_2, φ_3, ... and the eigenvalue λ. For the solution of wave equation, (7.21a) is modified as

$$\varphi_{i,j}^{n+1} = \varphi_{i,j}^{n} + \frac{\Omega_0 R_{i,j}^{n+1}}{\left(4 - h^2 k_c^2\right)} \tag{7.84}$$

Since we start with an assumed value of k_c, it needs to be updated from one iteration to the next. When we have the exact value of $\varphi_{i,j}^{n}$, the value of k_c can be determined from (7.70) yielding

$$k_c^2 = -\frac{\nabla_t^2 \varphi}{\varphi}, \qquad \nabla_t^2 = \frac{\partial^2}{\partial x^2} + \frac{\partial^2}{\partial y^2} \tag{7.85}$$

This expression is applied at each node (i, j). Since $\varphi_{i,j}^{n}$ is known only approximately, the value of k_c may vary from node to node. One may take the average of k_c over all the free nodes and use this value for the next iteration. A better choice than (7.85) is its weighted average with respect to φ [26]. Expression for this average is obtained by multiplying (7.70) with φ and integrating over the cross-section; one obtains

$$k_c^2 = \frac{-\iint_S \varphi \nabla_t^2 \varphi \, ds}{\iint_S \varphi^2 \, ds} \tag{7.86}$$

This expression is called the Rayleigh formula, and it is found to be variational in nature [6, 14].

Now we replace $\nabla_t^2 \varphi$ by its finite difference equivalent based on (7.9) and carry out the integration using the discrete values of $\varphi_{i,j}^{n}$, resulting in

$$k_c^2 h^2 = \frac{-\sum_{i=1}^{N}\sum_{j=1}^{M} \varphi(i,j)\left[\varphi(i,j+1) + \varphi(i,j-1) + \varphi(i+1,j) + \varphi(i-1,j) - 4\varphi(i,j)\right]}{\sum_{i=1}^{N}\sum_{j=1}^{M} \varphi^2(i,j)} \tag{7.87}$$

where the summation is carried out over all the free nodes in the device geometry. We use this value of k_c to update (7.84) and continue the iterations until convergence is reached. The cutoff wavelength for the mode is obtained from the final value of $(k_c h)^2$ as

$$(k_c h)^2 = \left(\frac{2\pi h}{\lambda_c}\right)^2 \tag{7.88}$$

We now apply this method to determine the cutoff wavelength of the ridge waveguide of Figure 7.26. The waveguide dimensions are $a_1 = 2$ cm, $b_1/a_1 = 0.5$, and the discretization used is $\Delta x = \Delta y = 0.01$ cm. The ridge parameters were varied as follows: $a_2/a_1 = 0.1$ to 0.9 in steps of 0.1, and $b_2/b_1 = 0.80$ to 0.95 in steps of 0.05. The computed cutoff wavelength for the dominant mode of the ridge waveguide λ_c' was normalized to the cutoff wavelength in the waveguide without ridge, $\lambda_c = 2a_1$. The software used was *waveguide.m*, and the results are plotted in Figure 7.27. It is seen that the λ_c' increases with increase in the ridge height b_2. It also increases with a_2 until it becomes maximum at $a_2/a_1 = 0.5$. The cutoff frequency for the dominant mode of the waveguide may therefore be decreased using a single ridge by a factor of about 3.8.

Once the cutoff wavenumber k_c is obtained from the analysis, it may be used to determine the propagation constant β for the mode by using $k_c^2 = k^2 - \beta^2$, where $k^2 = \omega^2\mu\epsilon$. The constant H_z lines for the dominant mode are plotted in Figure 7.28, and are similar to the electric field lines for the mode. This plot may be employed for diagnostics of the data.

The FDM is a very simple, versatile, but inefficient method. It requires large node density for accurate results. The asymptotic value corresponding to the zero discretization size may be obtained by extrapolating the data obtained for decreasing discretization size [6]. The extrapolation technique is discussed in Chapter 6. The basic concepts of finite difference method are utilized in the time-domain finite-difference method discussed in the next chapter.

7.4 Summary

The finite difference method is a simple and versatile differential equation solver. However, its efficiency is poor because the node density required for accurate

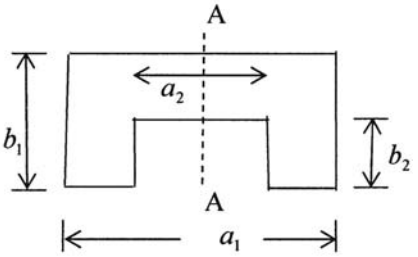

Figure 7.26 Cross-section of a ridged waveguide.

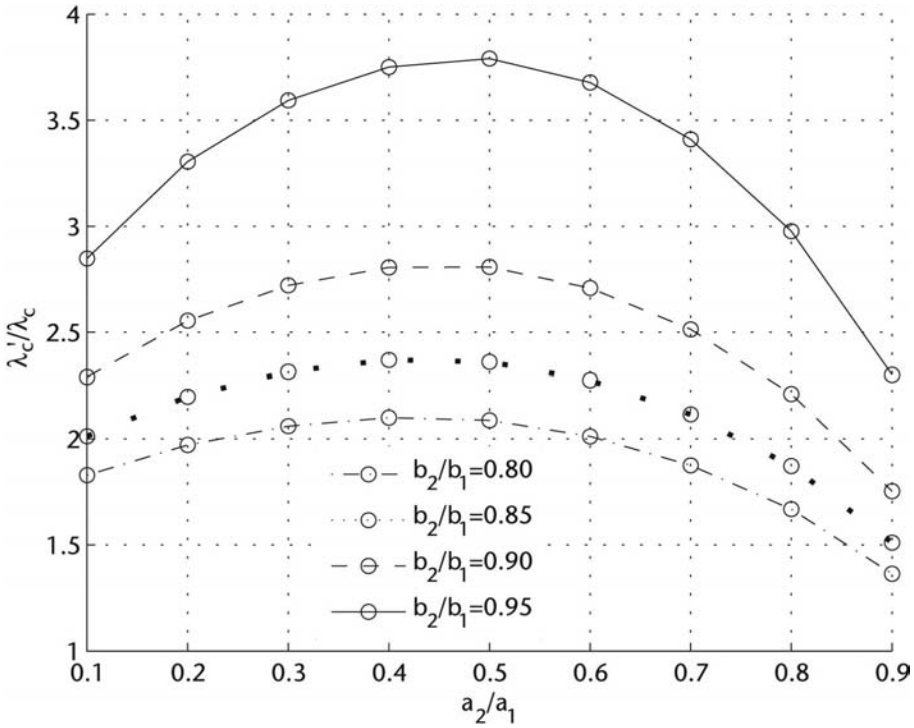

Figure 7.27 Ratio of the cutoff wavelength of the ridge waveguide λ_c' and the corresponding rectangular waveguide without ridge $\lambda_c(a_1 = 2$ cm, $b_1/a_1 = 0.5)$, $\Delta x = \Delta y = 0.01$ cm.

solution is more than 20. For the application of this method, the derivatives in the differential equation are expressed in the finite difference form resulting in an algebraic equation. This equation is applied at each node after the discretization of the device geometry. Some of the nodes are called fixed nodes because the value at these nodes is determined by the boundary conditions or excitation. The other nodes are called free nodes at which the potential values are obtained from the solution of simultaneous equations. The matrix equation is solved using iterative methods because the size of the matrix obtained for accurate solution is very large. Successive over relaxation may be used to reduce the number of iterations considerably. A simple expression is given to determine the optimum value of relaxation factor. Various types of boundary conditions one may come across while attempting FDM solution, like node on the interface, magnetic wall boundary condition, and node on a corner, are analyzed and expressed in finite difference form. The FDM is illustrated by its application to problems like inhomogeneously filled parallel plate capacitor, microstrip line, and rectangular and ridge waveguide. The effect of discretization on the accuracy of the solution is addressed through numerical dispersion determination. Examples are so designed that FDM analysis is carried out in a tutorial fashion without the use of software. For this the size of the problem is kept small through crude discretization and the use of symmetry conditions. The same problem is next worked out using the software and fine discretization to obtain accurate results.

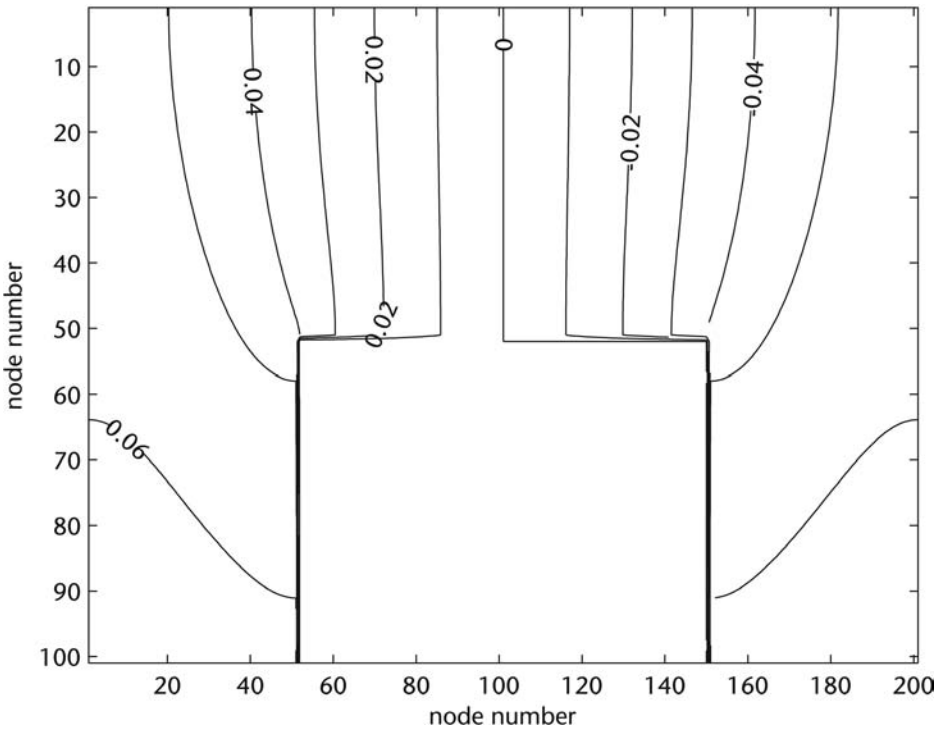

Figure 7.28 Plot of constant H_z contours for the dominant mode. The parameters are: $a_2/a_1 = 0.5$, $b_2/b_1 = 0.5$, $a_1 = 0.02$m, $b_1/a_1 = 0.5$.

References

[1] Green, H. E., "The Numerical Solution of Some Important Transmission-Line Problems," *IEEE Trans. Microwave Theory Tech.*, Vol. MTT-13, 1965, pp. 676–692.

[2] Iskander, M. F., et al., "A New Course on Computational Methods in Electromagnetics," *IEEE Trans. Educ.*, Vol. 31, 1988, pp. 101–115.

[3] Schneider, M. V., "Computation of Impedance and Attenuation of TEM-Lines by Finite Difference Methods," *IEEE Trans. Microwave Theory Tech.*, Vol. MTT-13, 1965, pp. 793–800.

[4] Sadiku, M. N. O., *Numerical Techniques in Electromagnetics*, Boca Raton, FL: CRC Press, 1992.

[5] Chari, M. V. K., and S. J. Salon, *Numerical Methods in Electromagnetism*, New York: Academic Press, 2000.

[6] Booton, R. C., *Computational Methods for Electromagnetics and Microwaves*, New York: John Wiley, 1992.

[7] Wexler, A., "Computation of Electromagnetic Fields," *IEEE Trans. on Microwave Theory Tech.*, Vol. MTT-17, 1969, pp. 416–439.

[8] Neff, H. P., Jr., *Basic Electromagnetic Fields*, 2nd ed., New York: Harper & Row, 1987.

[9] de Vahl Davis, G., *Numerical Methods in Engineering and Science*, New York: Van Nostrand Reinhold, 1986.

[10] "Computer-Oriented Microwave Practices," special issue of *IEEE Trans. on Microwave Theory and Techniques*, Vol. MTT-17, No. 8, August 1969.

[11] Vemuri, V., and W. J. Karplus, *Digital Computer Treatment of Partial Differential Equations*, Englewood Cliffs, NJ: Prentice-Hall, 1981.

[12] Metcalf, W. S., "Characteristic Impedance of Rectangular Transmission Lines," *Proc. IEE*, Vol. 112, 1965, pp. 2033–2039.

[13] Gupta, R. R., "Accurate Impedance Determination of Coupled TEM Conductors," *IEEE Trans. Microwave Theory Tech.*, Vol. MTT-17, 1969, pp. 479–489.

[14] Yamashita, E., et al., "Characterization Method and Simple Design Formulas of MDS Lines Proposed for MMIC's," *IEEE Trans. on Microwave Theory Tech.*, Vol. MTT-35, 1987, pp. 1355–1362.

[15] Molberg, J. R., and D. K. Reynolds, "Iterative Solutions of the Scalar Helmholtz Equations in Lossy Regions," *IEEE Trans. on Microwave Theory Tech.*, Vol. MTT-17, 1969, pp. 460–477.

[16] Davies, J. B., and C. A. Muilwyk, "Numerical Solution of Uniform Hollow Waveguides with Boundaries of Arbitrary Shape," *Proc. IEEE*, Vol. 113, 1966, pp. 277–284.

[17] Hornsby, J. S., and A. Gopinath, "Numerical Analysis of a Dielectric-Loaded Waveguide with a Microstrip Line-Finite-Difference Methods," *IEEE Trans. on Microwave Theory Tech.*, Vol. MTT-17, 1969, pp. 684–690.

[18] Beubien, M. J., and A. Wexler, "An Accurate Finite-Difference Method for Higher-Order Waveguide Modes," *IEEE Trans. on Microwave Theory Tech.*, Vol. MTT-16, 1968, pp. 1007–1017.

[19] Collins, J. H., and P. Daly, "Calculations for Guided Electromagnetic Waves Using Finite-Difference Methods," *J. Electronics & Control*, Vol. 14, 1963, pp. 361–380.

[20] Muilwyk, C. A., and J. B. Davies, "The Numerical Solution of Rectangular Waveguide Junctions and Discontinuities of Arbitrary Cross Section," *IEEE Trans. on Microwave Theory Tech.*, Vol. MTT-15, 1967, pp. 450–455.

[21] Sinnott, D. H., et al., "The Finite Difference Solution of Microwave Circuit Problems," *IEEE Trans. on Microwave Theory Tech.*, Vol. MTT-17, 1969, pp. 464–478.

[22] Corr, D. G., and J. B. Davies, "Computer Analysis of the Fundamental and Higher Order Modes in Single and Coupled Microstrip," *IEEE Trans. Microwave Theory Tech.*, Vol. MTT-20, 1972, pp. 669–678.

[23] Sandy, F., and J. Sage, "Use of Finite Difference Approximations to Partial Differential Equations for Problems Having Boundaries at Infinity," *IEEE Trans. on Microwave Theory Tech.*, Vol. MTT-29, 1981, pp. 484–486.

[24] Jordon, R. K., and S. H. Hook, "A Finite Difference Approach that Employs an Asymptotic Boundary Condition on a Rectangular Outer Boundary for Modeling Two-Dimensional Transmission Line Structures," *IEEE Trans. on Microwave Theory Tech.*, Vol. 41, 1993, pp. 1280–1286.

[25] Chang, C. N., Y. C. Wong, and C. H. Chen, "Hybrid Quasistatic Analysis for Multilayer Coplanar Lines," *IEE Proc.-H*, Vol. 138, 1991, pp. 307–312.

[26] Peterson, A. F., S. L. Ray, and R. Mittra, *Computational Methods for Electromagnetics*, New York: IEEE Press, 2001.

[27] Naiheng, Y., and R. F. Harrington, "Characteristic Impedance of Transmission Lines with Arbitrary Dielectric Under the TEM Approximation," *IEEE Trans. on Microwave Theory Tech.*, Vol. MTT-34, 1986, pp. 472–475.

[28] Kim, W., M. F. Iskander, and C. M. Krowne, "Modified Green's Function," *IEEE Trans. on Microwave Theory Tech.*, Vol. 55, 2007, pp. 402–408.

Problems

P7.1. Consider the trough problem discussed in Example 7.1. Use a 6×6 set of square cells to determine the potentials at the nodes for a given tolerance. Next, increase the number of cells to 12×12 and again determine the potential distribution

for the same tolerance. Compare your computed values with those given by (7.20) and comment on the accuracy of the solution with the decrease in cell size.

P7.2. Consider the trough shown in Figure 7.29. The lower half of the trough is filled with a dielectric having $\epsilon_r = 3$ and the upper half with $\epsilon_r = 1$. Show that the solution based on finite-difference method (FDM) is [7]

$$\varphi_1 = 0.3929V_0 \qquad \varphi_2 = 0.4777V_0 \qquad \varphi_4 = 0.0938V_0$$
$$\varphi_5 = 0.1250V_0 \qquad \varphi_7 = 0.0357V_0 \qquad \varphi_8 = 0.0491V_0$$

P7.3. The geometry of a shielded strip line is shown in Figure 7.30. Determine the potential distribution and the characteristic impedance of the line Z_0 with w/b = 0.8, t/b = 0, 0.1, 0.2, and 0.3, s/b = 0.1 to 0.7 in steps of 0.1 [3]. Plot the potential

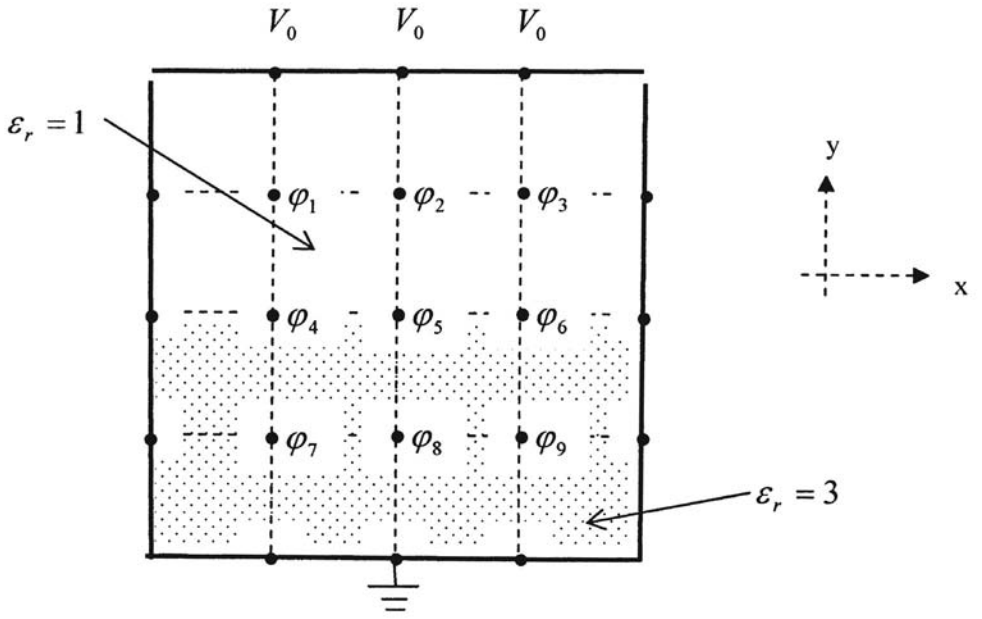

Figure 7.29 Geometry of a trough filled inhomogeneously with dielectric.

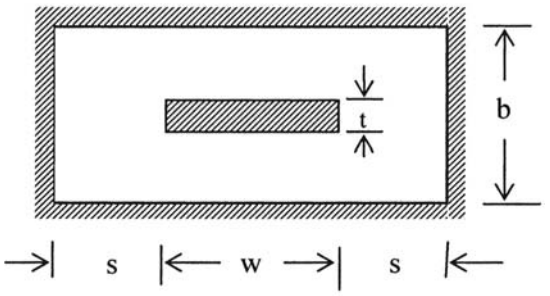

Figure 7.30 Cross-section of shielded strip line.

distribution in the cross-section. You may use the symmetry of the structure about the width and height to reduce the problem domain to its quarter and use the Neumann boundary conditions at the symmetry planes. Compare the results for $w/b = 1.5$, $(2s + w)/b = 4$ with the laterally open strip line case solved using MoM (Section 11.2.2). MoM result is 47.92 ohms for $w/b = 1.5$, $\epsilon_r = 1$. The FDM result is 47.12 ohms for $L/W = 3$ (using *mstrip.m*).

P7.4. Square coaxial line is a configuration similar to that given in Figure 7.30. Consider the coaxial line shown in Figure 7.31. Using the symmetry considerations, the problem can be reduced to one-fourth of its size. Show that

$$\varphi_1 = 140/322 V_0 \qquad \varphi_2 = 56/322 V_0 \qquad \varphi_3 = 91/322 V_0$$
$$\varphi_4 = 42/322 V_0 \qquad \varphi_5 = 21/322 V_0$$

Also, show that the capacitance per unit length of the line is given by

$$C_0 = 4\epsilon \frac{V_0 - \varphi_1}{V_0} = 2.26\epsilon$$

where ϵ is the dielectric constant of the medium filling the space between two conductors [7].

P7.5. The geometry of a suspended coupled strip line is shown in Figure 7.32. Determine the characteristic impedance of the line for $a = 5.0$ cm, $b = 5.0$ cm, $h = 1.0$ cm, $w = 2.0$ cm, $t = 0.001$ cm, $\epsilon_1 = \epsilon_0$, and $\epsilon_2 = 2.35\epsilon_0$. The reported impedance value is 65.02. The geometry of Figure 7.32 can propagate two different modes depending on the potential at the strips. If the strips are at the same potential, the mode of propagation is called the even mode. The symmetry plane parallel to

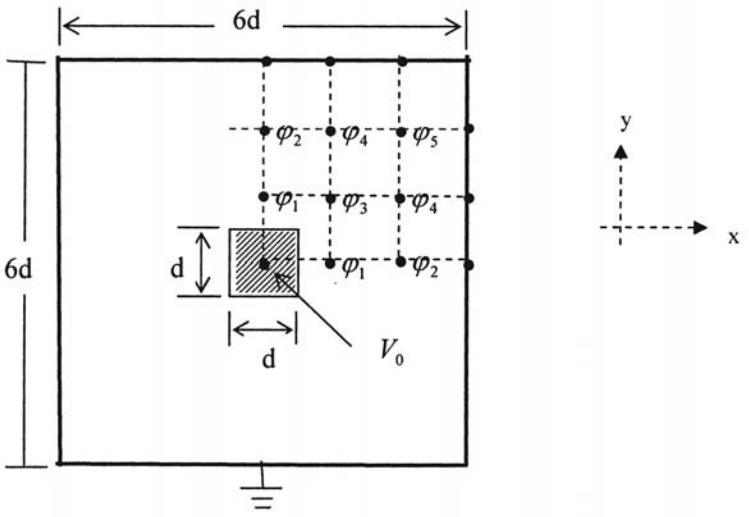

Figure 7.31 Cross-section of square coaxial line.

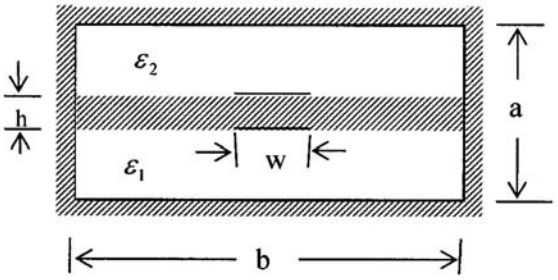

Figure 7.32 Cross-section of suspended coupled strip line.

the strips and passing through the substrate is the magnetic wall. When the strips are at different potentials, the mode of propagation is called the odd mode and the symmetry plane is the electric wall or ground plane. Placing this symmetry plane will convert the given geometry into a microstrip line geometry. Another symmetry consideration will reduce the problem to one-quarter size [27].

P7.6. The geometry of a coaxial line with circular inner conductor and rectangular outer conductor is shown in Figure 7.33. Determine the characteristic impedance of the line for $a = 1.0$ cm, $b = 1.25$ cm, $d = 0.51$ cm, and $\epsilon = \epsilon_0$. The reported impedance value is 50.43 ohms. You may use symmetry considerations to reduce the size of the problem [27].

P7.7 Solve the following wave equation:

$$\frac{\partial^2 \varphi}{\partial x^2} - \frac{1}{c^2}\frac{\partial^2 \varphi}{\partial t^2} = 0, \qquad 0 < x < 1, \qquad t \geq 0$$

subject to the boundary conditions

$$\varphi(0, t) = 0 = \varphi(1, t), \qquad t \geq 0$$

and the initial conditions

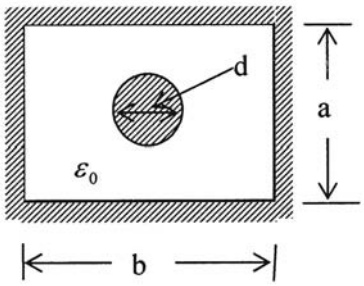

Figure 7.33 Cross-section of a coaxial line with circular inner conductor and rectangular outer conductor.

$$\varphi(x, 0) = \sin(\pi x), \qquad 0 < x < 1$$

$$\frac{\partial \varphi(x, 0)}{\partial t} = 0, \qquad 0 < x < 1$$

Compare your solution with the analytical value obtained from

$$\varphi(x, t) = \sin(\pi x)\cos(\pi c t)$$

Fortran code for a similar wave equation problem is available in [4].

P7.8. Solve the following Poisson equation:

$$\frac{\partial^2 \varphi}{\partial x^2} + \frac{\partial^2 \varphi}{\partial y^2} = -\frac{\rho_s}{\epsilon_0}, \qquad 0 \le x, y \le 1$$

subject to the boundary conditions

$$\varphi(x, 0) = 0\text{V}; \qquad \varphi(0, y) = -10\text{V}; \qquad \varphi(1, y) = 10\text{V}; \qquad \varphi(x, 1) = 20\text{V}$$

Assume $\rho_s = x(y - 1) \times 10^{-9}$ C/m^2, divide the region into 4×4 cells, and plot the potential at the free nodes. You may use successive over-relaxation. The analytical solution to this problem may be obtained by using (7.21) and superposition. If φ_1 is the solution to the Laplace equation $\nabla^2 \varphi_1 = 0$ subject to the boundary conditions given above, and φ_2 is the solution to the Poisson equation $\nabla^2 \varphi_2 = -\rho_s/\epsilon_0$ subject to $\varphi_2 = 0$ at $x = 0, 1$; $y = 0, 1$, then

$$\varphi = \varphi_1 + \varphi_2$$

where φ_2 is obtained by the eigenfunction expansion method and is given by

$$\varphi_2 = \sum_{m=1}^{\infty} \sum_{n=1}^{\infty} A_{mn} \sin\left(\frac{m\pi x}{a}\right) \sin\left(\frac{n\pi y}{b}\right)$$

with

$$A_{mn} = -\int_0^a \int_0^b \frac{\rho_s}{\epsilon_0} \sin\left(\frac{m\pi x}{a}\right) \sin\left(\frac{n\pi y}{b}\right) dx\, dy$$

For the given problem $a = 1$, $b = 1$ and $\rho_s = x(y - 1) \times 10^{-9}$ C/m^2, one obtains

$$A_{mn} = \frac{1 - (1 - (-1)^n)}{(m\pi)^2 + (n\pi)^2} \frac{144(-1)^{m+n}}{mn\pi} = \frac{-1}{(m\pi)^2 + (n\pi)^2} \frac{144(-1)^{m+n}}{mn\pi}, \text{ for } n \text{ odd}$$

The Fortran source code based on SOR and the solution is available in [4].

P7.9. Use FDM to solve the following one-dimensional scalar Helmholtz equation:

$$\frac{d^2E_y(x)}{dx^2} + Ck^2E_y(x) = 0$$

where $k = 2\pi/\lambda$ defines the wavelength in the medium. Show that the value of C such that the propagation constant β in the discretized medium is equal to k, the propagation constant in the continuous medium, is given by the expression

$$C = \left(\frac{\sin\left(\frac{k\Delta x}{2}\right)}{\frac{k\Delta x}{2}} \right)^2$$

Calculate C for $\Delta x/\lambda$ = 1/8, 1/12, 1/20, and 1/40 and compare with the values obtained in Problem 7.10.

P7.10. The field distribution in a transmission line resonator is described by the following scalar wave equation:

$$\frac{d^2E_y(x)}{dx^2} + \pi^2E_y(x) = g(x), \qquad 0 < x < 1$$

with the boundary conditions

$$E_y = 0 \text{ at } x = 0 \text{ and } x = 1$$

Assume the resonator length to be 1m and therefore the resonant frequency is 150 MHz. Now discretize the wave equation and use finite difference approximation to obtain the following expression for the ith cell:

$$2E_y(i) - E_y(i-1) - E_y(i+1) - (\pi\Delta z)^2E_y(i) = g(i)$$

To fine tune the resonator and to determine the phase velocity in the discretized domain, we introduce a correction factor C in the above expression to give

$$2E_y(i) - E_y(i-1) - E_y(i+1) - C(\pi\Delta z)^2E_y(i) = g(i)$$

Assume $g(i) = 1$ at the central cell and 0 for others. Tune the resonator to 150 MHz by varying C for three different cell sizes Δx = 0.25m, 0.2m, and 0.1m. Determine the amplitude distribution over the resonator as a function of C. Interpret the results in terms of phase velocity of the wave (see also Section 10.2.2).

P7.11 (a) Derive the finite difference implementation of the boundary condition $D_{in} = D_{2n}$ for V_0 located on the dielectric boundary as shown in Figure 7.6.

(b) Derive the finite difference implementation of the symmetry condition $\partial V/\partial n = 0$ along the y-axis as shown in Figure 7.34.

P7.12 Consider the rectangular waveguide of Figure 7.24 with $b = a/2$. The waveguide is half filled with a dielectric of $\epsilon = \epsilon_0 \epsilon_r$ so that the nodes 1, 2, 3, . . . are on the interface as shown in Figure 7.35. We are interested in finding the approximate closed-form expression for the cutoff wavelength for the dominant TE_{10} mode. For this we use symmetry condition about $x = a/2$ plane and coarse discretization to model the problem as shown. The potential function φ represents H_z field for the TE mode. Therefore, the boundary conditions are: $\varphi = 0$ at 13, 3, and 8. Also assume that $\varphi_6 = \varphi_{11} = \varphi_1$ and $\varphi_{12} = \varphi_7 = \varphi_2$ for the mode. Show that the cutoff wavelength λ_c for $h = a/4$ is given by

$$\lambda_c = \frac{\pi a}{2} \frac{\sqrt{\epsilon_r + 1}}{\sqrt{\left(4 - \sqrt{2}\right)(\epsilon_r + 1) - 4}}$$

where a is the width of the waveguide.

P7.13. Consider a square waveguide with dimension $b = a$ as shown in Figure 7.36(a). Use FDM to determine the approximate solution for the cutoff wavelength for the dominant TM_{11} mode. For this we use symmetry conditions about $x = a/2$

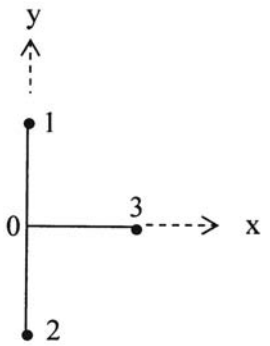

Figure 7.34 Geometry of nodes with Neumann boundary condition.

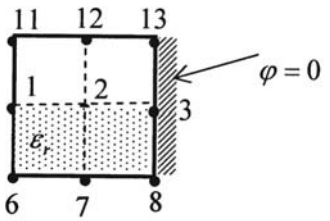

Figure 7.35 Geometry of a rectangular waveguide half filled with dielectric and symmetry condition employed.

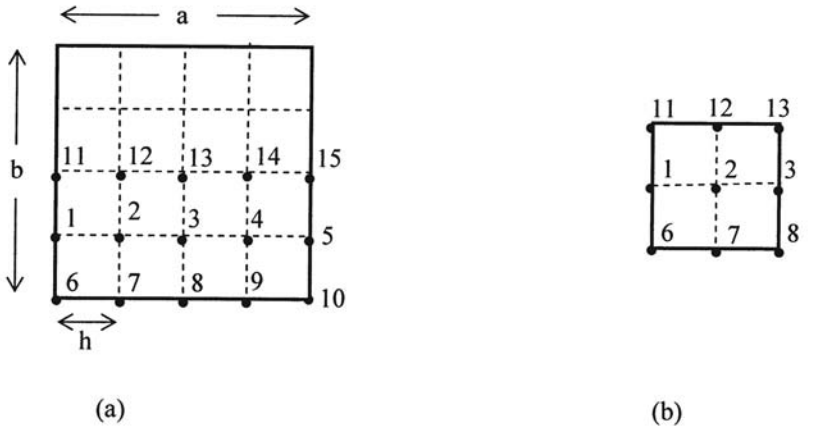

Figure 7.36 Geometry of a square waveguide: (a) discretized waveguide geometry; and (b) waveguide with two-fold symmetry.

and $y = b/2$ planes and coarse discretization with square grid to model the problem as shown in Figure 7.36(b). The potential function φ represents E_z field for the *TM* mode. Therefore, the boundary conditions are: $\varphi = 0$ at 11, 1, 6, 7, and 8; and $\partial\varphi/\partial n = 0$ at 12, 13, and 3. Show that the eigenvalues are given by $\lambda = \pm 2\sqrt{2}$, and for $h = a/4$ the cutoff wavelength λ_c for the mode is obtained as $\lambda_c = 1.4517a$ compared with the exact value of $1.414a$, an error of less than 3%.

P7.14. Consider a rectangular waveguide of dimension $a \times b$, and $b = a/2$. Determine the cutoff wavenumber k_c for the TM_{11} mode using FDM. Use $\Delta x = a/2$, $\Delta y = b/2$ for the discretization of the geometry. Compare with the analytical solution $k_c = \pi\sqrt{\left(\frac{1}{a^2} + \frac{1}{b^2}\right)}$. You may use $a = 2$ cm for comparison.

P7.15. Consider a parallel plate capacitor inhomogeneously filled with the dielectric as shown in Figure 7.37. The upper plate is charged to 1 volt and the lower plate is grounded. The boundary conditions therefore are: $\varphi_i = 0$ for $i = 1$ to 7, and $\varphi_i = 1$ for $i = 15$ to 21. The side walls of the capacitor are terminated in magnetic

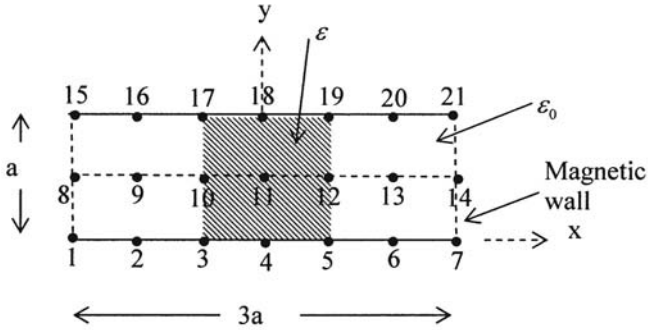

Figure 7.37 Geometry of a parallel plate capacitor inhomogeneously filled with dielectric.

walls to limit the size of FDM domain. The geometry is discretized as shown with $\Delta x = \Delta y = a/2$. Determine the capacitance per unit length. Compare the computed capacitance with the analytical value $C = (2\epsilon_0 + \epsilon)$.

P7.16. The singularity of charge density distribution on the metal strips in planar lines is principally determined by the dielectric configuration below the strip. In CPW line, the charge distribution is similar to the one that shown in Figure 7.18 if the substrate is single layered. Let us now introduce two thin dielectric layers between the main substrate and the metal strip as shown in Figure 7.38. Determine the charge density distribution on the central strip and show that the increase in density towards the edges is almost linear for $w = 30$ μm, $s = 15$ μm, $\epsilon_{r1} = 3.8$, $\epsilon_{r2} = 440(1 - j0.01)$, and $\epsilon_{r3} = 23.5$ [28].

P7.17. Use FDM to solve the following differential equation for the box shown in Figure 7.39:

$$\frac{\partial^2 V}{\partial x^2} + \frac{\partial^2 V}{\partial y^2} + 50 = 0, \qquad 0 \le x, y \le 1$$

subject to the boundary conditions $V = 10$ at $x = 0, 1$; $\partial V/\partial y = 40$ at $y = 0$, and $\partial V/\partial y = -20$ at $y = 1$. Assume $\Delta x = \Delta y = h = 1/3$ and

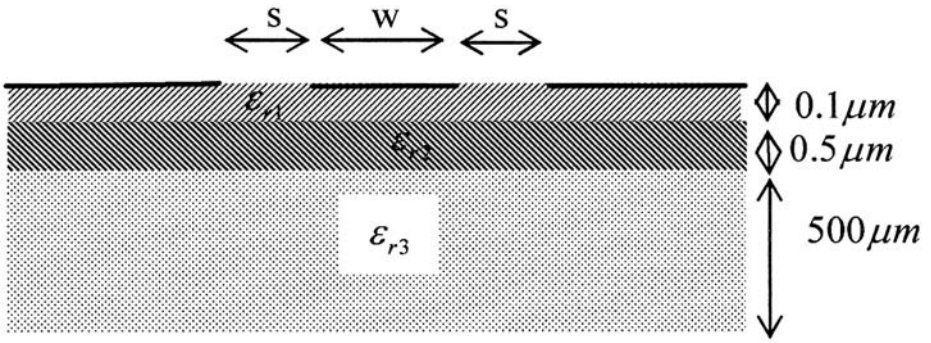

Figure 7.38 A multilayered CPW geometry.

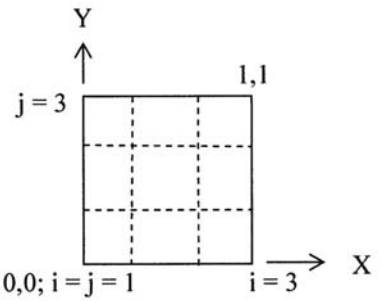

Figure 7.39 Discretized rectangular box geometry.

1. Obtain an expression for $V(i, j)$ in terms of the values at the four nodes surrounding it.
2. To implement the boundary condition at $y = 0$, obtain an expression for $V(i, 1)$ in terms of values at the nodes surrounding it.
3. To implement the boundary condition at $y = 1$, obtain an expression for $V(i, 4)$ in terms of values at the nodes surrounding it.
4. How can you reduce the number of unknowns? Write down the final matrix equation to be solved.
5. Develop a computer code to solve the same problem using $h = 0.05$, 0.1, 0.2, 0.25, and 0.5.